Nanoscale Research Letters

REVIEW Open Access

Photodynamic Therapeutic Effect of Nanostructured Metal Sulfide Photosensitizers on Cancer Treatment

Daysi Diaz-Diestra[1,2], Hanna Madadi Gholipour[3], Marjan Bazian[4], Bibek Thapa[5] and Juan Beltran-Huarac[6*]

Abstract

Photodynamic therapy (PDT) utilizes photosensitizers (PSs) to produce reactive oxygen species (ROSs) upon irradiation, which causes the shutdown of vessels and deprives the tumor of nutrients and oxygen, and in turn induces adverse effects on the immune system. However, significant efforts are needed to increase the efficiency in PDT in terms of light delivery to specific PSs for the clinical treatment of tumors located deep under the skin. Even though PDT offers a disease site-specific treatment modality, current efforts are directed to improve the solubility (in body fluids and injectable solvents), photostability, amphiphilicity (for tissue penetration), elimination, and systemic toxicity of traditional PSs based on porphyrin derivatives. Nanostructured materials show promising features to achieve most of such combined efforts. They can be artificially engineered to carry multiple theranostic agents onto targeted tumor sites. However, recent studies on photosensitive Cd-based nanostructures, mostly used in PDT, indicate that leeching of Cd^{2+} ions is stimulated when they are exposed to harsh biological conditions for continuous periods of time, thus making them acutely toxic and hindering their applications in in vivo settings. Since nanostructured materials are not completely immune to degradation, great strides have been made to seek new alternatives. In this review, we focus on the latest advances of Cd-free nanostructured metal transition sulfides (MTSs) as alternative PSs and study their high-energy transfer efficiency, rational designs, and potential applications in cancer-targeted PDT. Nanostructured MTSs are discussed in the context of their versatility to serve as phototherapy agents and superior properties, including their strong absorption in the NIR region, excellent photothermal conversion efficiency, controlled reactive oxygen species (ROS) production, versatile surface chemistry, high fluorescence, and structural and thermal stability. We discuss the latest advancements in correlating the self-aggregation of MTSs with their passive tumor cell targeting, highlighting their ability to efficiently produce ROSs, and mitigating their dark toxicity through polymeric functionalization. Treatment of deep-seated tumors by using these PSs upon preferential uptake by tumor tissues (due to the enhanced permeability and retention effect) is also reviewed. We finally summarize the main future perspectives of MTSs as next-generation PSs within the context of cancer theranostics.

Keywords: Photodynamic therapy, Metal sulfides, Photosensitizers, Cancer treatment

Introduction

Cancer, a tumor or malignant growth arising from the division of abnormal cells, has caused an estimated 19.3 million new cancer cases (18.1 million excluding nonmelanoma skin cancer) and almost 10.0 million cancer deaths (9.9 million excluding nonmelanoma skin cancer) occurred in 2020, according to recent estimates of the worldwide mortality rate released by the International

*Correspondence: beltranhuaracj19@ecu.edu
[6] Department of Physics, Howell Science Complex, East Carolina University, Greenville, NC 27858, USA
Full list of author information is available at the end of the article

Agency for Research on Cancer [1]. The deaths are projected to rise to 28.4 million in 2040. The most diagnosed cancers are lung (2.2 million), breast (2.3 million), and colorectal (1.9 million) [1]. Facing this statistical catastrophe through regular prevention-focused approaches and early intervention programs falls short of patients' expectations, who demand therapeutic alternatives to be affordable, side-effect discriminated, and more efficient and effective. Among the existing cancer treatments are surgery, chemotherapy, radiation therapy, targeted therapy, immunotherapy, laser treatment, stem cell transplant, hyperthermia, and small molecule-based therapy, being those of immunosuppressive-type most commonly used [2, 3]. However, although chemotherapy and ionizing radiation can destroy malignant growths at sufficient drug/radiation doses, they are noxious to the bone barrow and provoke immunostimulatory effects such as induction of heat-shock proteins [4]. In addition, cumulative radiation doses are restricted in radiation therapy, whereas systemic side-effects are still an issue in chemotherapy [5]. It has also been observed a substantial reduction of the natural killer cell function and diminution of lymphocytes in surgical resection of tumors, which are accompanied by high recurrence rates [6, 7] Thus, the desired cancer therapy must surmount these hurdles, and not only annihilate the main tumors but also recognize, localize and destroy any surrounding cancerous cells (even at distant micrometastases) by simultaneously setting off the immune system [8, 9].

Photodynamic therapy (PDT) is a versatile oncologic therapeutic modality and has been widely used clinically due to its intrinsic minimal noninvasiveness and high selectivity that enable to minimize the adverse impact on healthy tissues [10–13]. PDT employs three major components—light, photosensitizer (PS), and molecular oxygen. The visible light excites the PS accumulated in cancer cells, and the excited PS transfers photon energy to surrounding molecular oxygen to produce reactive oxygen species (ROS) that leads to death of cancer cells [12, 14, 15]. The PDT offers excellent repeatability without cumulative toxicity, low long-term morbidity, desired functional and cosmetic outcomes, and enhanced quality of life of patients [7]. The therapeutic efficacy of PDT greatly relies on properties of the PS such as aqueous solubility, greater tumor selectivity, high chemical purity, strong photosensitivity, and light absorption rate [11]. The idealization of PDT dates back to the early beginning of twentieth century, when a German medical student, Oskar Raab, serendipitously found that infusoria and species of *Paramecium caudatum* could be killed, when exposed to sunlight in the presence of a cell-specific dye called acridine [16, 17]. This was the first report on how PDT uses PS and since then, several varieties of synthetic (aniline dyes, eosin, fluorescein, etc.) and natural (*L. racemose*, Rose Bengal, *A. procera*, etc.) drugs have been developed as PSs [12]. To date, more than thousands of PSs, including natural and synthetic, are reported [18–20].

The first-generation PSs, such as hematoporphyrin derivative (HpD) and photofrin, and second-generation PSs, such as benzoporphyrins, purpurins, texaphyrins, and protoporphyrin IX (PpIX), have received extensive clinical uses [21]. However, most of these PSs possess complex composition and have low light absorption rate. Further, poor water solubility of these PSs precipitates aggregation, leading to quenching effect [21]. Currently, there are active research in progress in the field of nanotechnology in developing PSs with greater tumor selectivity, enhanced hydrophilicity, and strong photosensitivity to yield a reliable photodynamic reaction. The studies show that metal nanoparticles such as gold, silver and copper, manganese, aluminum nanoparticles; organic–inorganic hybrid nanoparticles, metal oxide nanoparticles, metal sulfide nanoparticles, Cd-free nanostructured metal chalcogenides (NMCs) have been extensively investigated in PDT [22–25]. While nanoparticles surface endows increased chemical activity, they require relatively low-power radiation to lead photo-stimulated reaction to generate singlet oxygen [26].

In this review, we discuss the recent development of Cd-free NMCs as alternative PSs and focus on the role of metal sulfide nanostructures in PDT for treatment of cancer. We consider metal sulfide nanomaterials for ROS generation to advance the photodynamic method. The recent developments in terms of high-energy transfer efficiency, rational designs, and potential applications of Cd-free NMCs in cancer-targeted PDT will be also discussed. We discuss the self-aggregation of NMCs in passive tumor cell targeting. The treatment of deep-seated tumors by using these PSs upon preferential uptake by tumor tissues due to the enhanced permeability and retention (EPR) effect, is also reviewed. We finally summarize the main future perspectives of NMCs as next-generation PSs within the context of cancer theranostics.

Fundamentals of Photodynamic Therapy

PDT includes the administration of a tumor-targeting PS drug followed by irradiation with visible light of particular wavelength corresponding to the absorption spectrum of the PS [20]. The energy of the excited PS is then transferred to molecular oxygen ($^3O_2$), which produces acutely-toxic singlet oxygen ($^1O_2$), a specific ROS, and superoxides. $^1O_2$ is crucial for inducing tumor cell ablation via oxidation of key cellular macromolecules [7, 27]. A depiction that summarizes the interaction of light with tissue that results in reflection, absorption, and scattering

is shown in Fig. 1. Selectivity in PDT depends on the degree of accumulation of the PS in the cancerous tissue and its vasculature, and on the restricted application of the incident light to the lesion zone. Out of the non-irradiated areas, the toxicity is minimal and can arise from the tissue tropism, due to daylight exposure or topical administration, that the PS shows [27, 28]. To date, the most widely used PS is photofrin, which is made up of purified aqueous mixtures of porphyrins [11]. This commercial PS has proven to be effective in certain neoplastic conditions, such as micro-invasive endo-bronchial non-small cell lung cancers, inoperable esophageal tumors, and neck and head malignancies [27, 29]. It has also been used in treating other types of cancer, including skin, superficial bladder, ovarian, breast, colon, and prostate [13, 30–32].

Photophysical and Photochemical Processes

PDT is an intrinsic, dynamic process of the interaction of light, PS, and oxygen. A proper coordination of the light source, light delivery and the PS is crucial for an effective therapeutic delivery in PDT [33]. The dynamic interaction processes can be categorized into (i) photophysical process—light–tissue interaction and light–PS interaction, and (ii) photochemical process [34]. The incident light interacts with optically inhomogeneous biological tissues upon the delivery of light, leading to attenuation of light energy due to reflection, scattering and absorption [35], as shown in Fig. 1.

The reflection and refraction (refraction is not shown in Fig. 1) occur at the interface between two media with mismatched refractive indices and are governed by Fresnel's law and Snell's law, respectively. The resulting loss of light intensity directly relates to the relative values of the refractive indices of the media. The intensity loss can be minimized by application of light in perpendicular direction [33]. Scattering of light in tissue is the most paramount interaction contributing to approximately 90–99% of the total light attenuation [36]. This results in dispersion of light (widening of light beam) and eventual loss of fluence rate, known as power per unit area of light in W m^{-2} [35]. While inelastic scattering (Raman scattering and Brillouin scattering) influences negligibly the PDT, elastic scattering such as Rayleigh scattering, and Mie scattering play a dominant role. The Rayleigh scattering is a more wavelength-dependent process and occurs when the size of atoms or molecules in tissue is much smaller than the light wavelength ($\lambda/10 >$ particle size, where λ is the light wavelength). In contrast, the Mei scattering is a non-wavelength selective process and occurs when the interacting molecules are comparable or larger than the light wavelength [37].

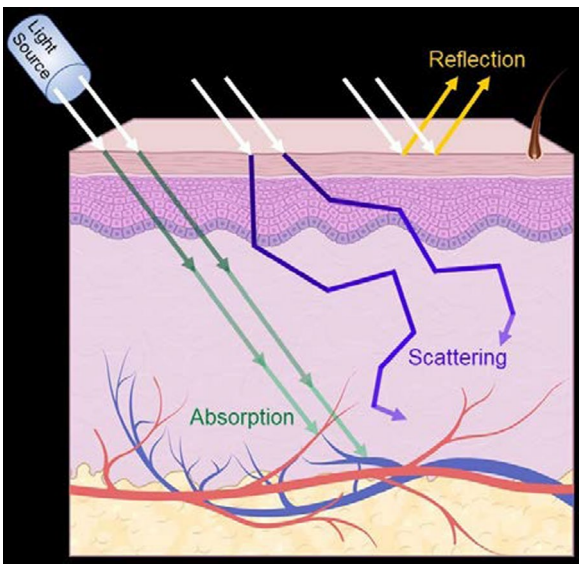

Fig. 1 Propagation of light in biological tissue. Interaction of light with tissue results in reflection, absorption, and scattering

The absorption of light in tissue occurs when the photon frequency matches the frequency associated with the molecule's transition energy and is influenced by the optical properties, size, shape, and density of the tissue elements [38]. Water, hemoglobin, melanin, cytochromes, elastin, and collagen are the major highly absorbing molecules in tissue. Together, absorption and scattering cause light attenuation resulting in loss of light intensity and leads to reduced scattering coefficient (μ_S) and absorption coefficient (μ_a) [33]. The light intensity (I_x) at given depth "x" in the tissue can be determined as $I_x = I_0 e^{-(\mu_a+\mu_S)x}$, where I_0 is the initial light intensity [34]. The effective penetration depth in PDT for solid tumors is defined as the depth "x" where I_x decreases to 37% of I_0. Most of the clinically used PSs show a Soret band at approximately 400 nm and multiple absorption peaks between 600 and 700 nm (Q-bands), which yields light penetration depth of approximately 3–5 mm depending on the tissue. Therefore, the use of PSs with absorption peaks at wavelength 700 nm or longer is preferred for deeper penetration of the light in tissue [38].

While a PS molecule in its ground singlet state (S_0) consists of paired electrons with total spin ($S = 0$) and multiplicity = 1, its exited singlet states (S_x, where $x = 1$, 2, 3, …with increasing energy state) are subdivided into multiple vibrational levels. The absorption of light by PS results in transfer of electrons to the short-lived (nanoseconds) exited singlet state. The electrons in the exited singlet state, eventually, fall to S_0 upon relaxation. According to the vibrational relaxation (VR), an electron in a higher vibrational level of an exited singlet state (e.g., S_1) promptly falls to lowest vibrational level of the excited

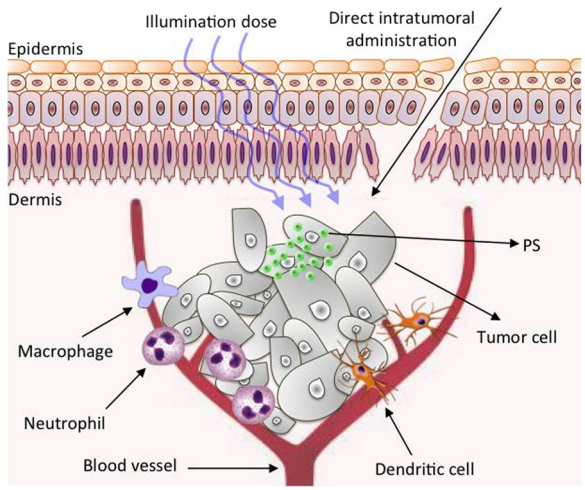

Fig. 2 Fundamental photodynamic therapy mechanism to treat shallow/deep tumors via intratumoral injection. Significantly modified from Ref. [9]

singlet state (S_1), dissipating heat energy. Following VR, the electron ultimately falls back to S_0 via fluorescence emission or release of heat. The emitted light possesses higher wavelength (or lower energy) than that of originally absorbed light. Also, the electrons from S_1 may be caught into long-lived (milliseconds) triplet excited state (T_1) in between the exited and ground singlet states due to a non-radiative process known as intersystem crossing, where the electrons are no longer paired with the ground state and possess parallel spin. A rapid and stepwise VR within the vibrational levels in T_1 can lead the electrons back to S_0, emitting phosphorescence [10, 34].

The excited PS then interacts directly with either surrounding $^3O_2$ (triplet ground state) to generate $^1O_2$ via energy transfer (~ 950 meV, type II), or any substrate to form free radicals via charge transfer (proton/electron, type I). The fundamental photodynamic therapy mechanism via intratumoral injection and the generation of reactive oxygen species and excited states are displayed in Figs. 2 and 3. In type I reaction, the free radicals may

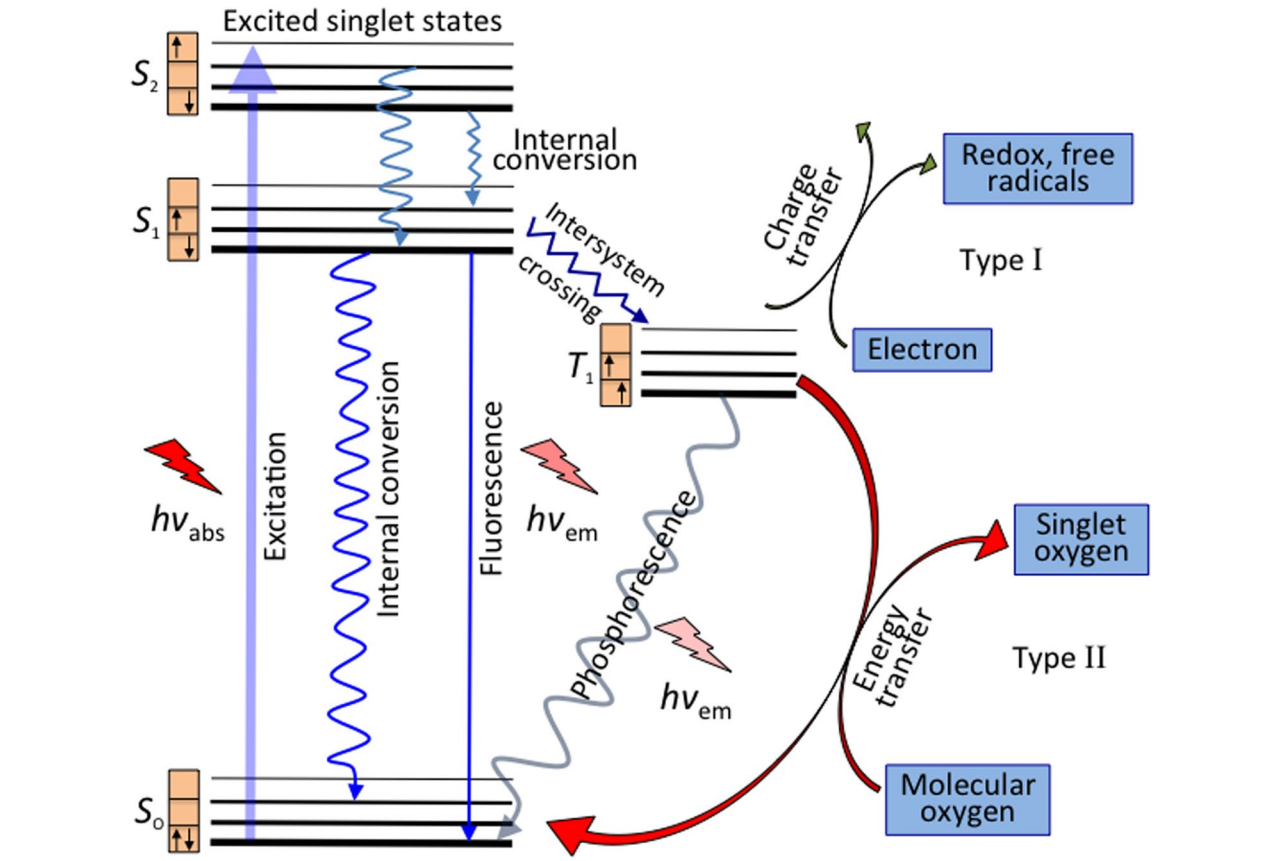

Fig. 3 Generation of reactive oxygen species and excited states of the photosensitizer. Light promotes the excitation of an electron from a low-energy singlet state (S_o) to high-energy singlet states ($S_{1,2}$). Such states can lose their energy via fluorescence (radiative emission, light) or internal conversion (non-radiative emission, heat). The spin flipping of the high-energy electron takes places via intersystem crossing, which leads to a long-lived excited triplet state (T_1). Type I and II reactions favor the formation of free radicals and singlet oxygen ($^1O_2$), respectively, in the presence of $^3O_2$. Significantly modified from Ref. [11]

further react with oxygen to produce ROS. Also, both reactions may take place simultaneously being their kinetics strongly favored by the oxygen, substrate concentration, and type of PS. Superoxide anion initially produced via type I pathway by monovalent reduction does not cause oxidative damage but reacts with itself to generate oxygen and hydrogen peroxide (H_2O_2), which is catalyzed by the enzyme superoxide dismutase [39]. Superoxide also promotes the donation of one electron to reduce metal ions, which act as catalyst to convert H_2O_2 into hydroxyl radical ·OH. Both H_2O_2 and ·OH are important in biological settings since most cells have metals, which facilitate such catalyst-based reaction, and they can easily pass through cell membranes and cannot be excluded from cells [8]. Highly reactive HO^- induces not only damage through rate-limited diffusion, but also add new radicals that react with other molecules in a chain reaction, which together with $^1O_2$ (produced by type II pathway) causes oxidative damage in lipids, fatty acids and DNA in areas proximal to the PS localization.

PDT Mechanism for Tumor Destruction

The PDT-induced tumor destruction primarily occurs both in apoptotic (programmed cell death) and necrotic (non-programmed cell death) pathways [10, 29]. The light-activated PS can exert its tumor destruction effect either through direct tumor cell killing (occlusion of the tumor-associated vasculature) or modulation of the immune system [26]. Regarding the first mechanism, ROS species generated by the photoexcitation of PSs cause the oxidation of the lipids, fatty acids, and DNA in areas proximal to the PS localization. This oxidation in turns induces irreversible damages into the cellular compartments (i.e., mitochondria, lysosomes, membrane) that leads to cell apoptosis, necrosis, or autophagy. These three mechanisms depend on a variety of parameters, including the nature of the PS applied, the PDT dose, as well as the genotype of the cells. For instance, high intensity light doses generally trigger necrosis, while low intensity trigger apoptosis [10]. On the other hand, if the PS is localized in the intracellular compartments the cell death will probably occur through an apoptotic pathway, while if the PS is localized in the plasma membrane or lysosomes, the cell will probably undergo a necrotic or an autophagic pathway.

The localization of the PS is also controlled by its surface properties. Hydrophobic compounds have been found to rapidly diffuse into the tumor cells and localized in the intracellular compartments compared to more polar compounds, which generally internalized through active processes that are slower and tend to localize on the outer cellular compartments. All these controllable factors allow to develop more personalized and efficient PDT treatments. The second proposed mechanism relies on the damage of the tumor vascular system. Similar to tumor cells, the vessels are abnormal and have poor and incomplete cellular borders [40] that facilitates the PS accumulation, which after activation causes a disruption in the vascular walls and cells, inhibiting the blood flow to the tumor decreasing the oxygen levels intake by the tumor (hypoxia) [41]. This event leads to necrosis of both tumor cells and vasculature, whose lysis stimulates the release of a high amount of intracellular debris that further blockage and collapse the micro vasculature feeding of the tumor [10, 42]. The PDT-treated dying cells (tumor cells and vasculature) also release different inflammatory mediators such as proteinases, peroxidases, cytokines, growth factors, and other inmunoregulators [9, 43], that activate an immune response (third mechanism). The initiation of this immune cascade attracts various immune cells, such as macrophages and neutrophils to the treatment region that further contribute to the tumor destruction by phagocytosing PDT damaged cancer cells and activating cytotoxic T cells and dendritic cells that induce necrosis or apoptosis whenever tumor cells are found [43, 44]. Although all these mechanisms combined or separated induce mechanistic cell toxicity, a more controlled cell killing process can be achieved by tailoring the properties of PSs.

Properties for Ideal Photosensitizers

PSs play a critical role in PDT to dictate how efficiently $^1O_2$ is generated. The PDT-induced anti-tumor effects and the treatment efficacy of PDT mainly rely on the properties of PSs. To enhance treatment efficacies, an ideal PS should possess the following properties: (1) high tumor selectivity and subcellular targeting capability; (2) strong absorption with high extinction coefficient at near-infrared (NIR) wavelength range (700–1300 nm), where tissue penetration is maximized and the auto-absorption is minimized by other endogenous molecules (including hemoglobin); (3) negligible dark toxicity; (4) high quantum yield of $^1O_2$ generation; (5) inexpensive and economically feasible; and (6) excellent aqueous solubility. As the development of novel PSs has been evolving, many of these properties were successfully attained which were used to sort them out. The first-generation PSs were developed in the 1970 that included porphyrin-based PSs [13]. These PSs were highly effective in first clinical trials, showing efficient tumor destruction, negligible dark toxicity and easy formulation in water-soluble preparations [7]. However, prolonged patient photosensitivity (poor clearance), low absorption of light ($e = 1170\ M^{-1}\ cm^{-1}$), and sub-optimal tumor selectivity have limited its use in PDT. In order to overcome these limitations, a second generation of PSs were developed

which included porphyrin derivatives, phthalocyanines, chlorins, anthraquinones, curcuminoids and its metalated derivatives (i.e., aluminum phthalocyanine tetrasulfonate and Si(IV)-naphthalocyanine). These PSs presented higher quantum yields of $^1O_2$, absorption at longer wavelengths (630–850 nm, providing deeper tissue penetration), shorter tissue accumulation, and cutaneous photosensitivity. Nevertheless, their poor tumor accumulation, aggregation, and self-quenching in aqueous solutions (as a result of their hydrophobicity) diminish their PDT efficacy. To tackle these drawbacks, PSs have been conjugated to biological targeting molecules, such antibodies, and peptides, or encapsulated in other carriers (e.g., polymers, micelles, and nanoparticles) leading to the third generation of PSs. This approach significantly increased the tumor selectivity and enables to minimize: (i) the damage of surrounding healthy tissues, (ii) side effects including prolonged skin photosensitivity, and (iii) invasiveness [11].

Nanoparticles in PDT

Recently, the use of nanoparticles (NPs) has been proposed as carriers of PSs due to their unique properties, such as (1) synthetic feasibility; (2) ease of functionalization with target moieties that increase PSs biodistribution, pharmacokinetics, cell uptake, and selectivity; (3) ability to transport hydrophobic drugs intravenously; (4) large volume distribution increasing high delivery of PSs into target sites; (5) easier internalization and retention into tumor tissues via the EPR effect given the tumor leaky vasculature; (6) controlled release of drugs; (7) protection of PSs against degradation and prolonged circulation in the bloodstream; and (8) versatility to incorporate other existing therapies or diagnosis modalities to PDT [7, 27, 45–47]. The use of NPs as cargo for PSs has been broadly divided into two categories: Biodegradable (natural or synthetic polymer-based NPs) and non-biodegradable (ceramic or metal-based NPs). Likewise, given that the distinct nanoformulations dictate the active intermediary role of NPs in the process of photodynamic activation, a new classification was proposed by Chatterjee et al., namely, as passive, and active nanocarriers [45]. In the latter, NPs participate in photodynamic process either as energy transducers or PSs themselves. In the former, nanostructures absorb the incident light at wavelengths transparent to the body and then transfer it to the PSs, thus allowing the possibility to treat deep-seated tumors. Some of the NPs used for this approach include upconversion NPs, noble metal NPs, metal sulfides/oxides, and carbon-based nanomaterials, which have shown to be relevant for in vitro and in vivo studies. Nevertheless, some major limitations of existing organic PSs (such as low extinction coefficients and poor photo-stability) pose a big challenge for clinical applications [11, 26].

In this sense, the innovation of inorganic nanostructures with the intrinsic ability to produce ROS upon the absorption of light has open new arenas for their use as PSs. Some of the first-evaluated inorganic NPs included TiO_2, ZnO, fullerene, and Cd-based quantum dots [48, 49]. Although these PSs compared to conventional organic PSs exhibit several advantages, some issues ascribed to low absorption at longer wavelengths have limited their translation to clinical applications. Recently, NIR-absorbing metal NPs (e.g., Au, Pd) have been evaluated as PSs due to its high biocompatibility and tunable surface plasmon resonance absorbance, which not only induces ROS production but can also generate light-to-heat conversion (photothermal effect). Their preparation, however, requires tedious and expensive synthetic procedures that increase their cost effectiveness. Moreover, their non-biodegradability raises toxicity concerns which further limits their clinical applications. Over the past few years, other metal NPs have been evaluated, e.g., NIR-absorbing copper sulfide (CuS) NPs due to its low cost and biodegradability. Previous reports indicate that these NPs possess low cytotoxicity, high photostability and photothermal conversion efficiency, intriguing photodynamic activity, tunable light absorption to longer wavelengths, higher molar extinction coefficients (at least 3–7 orders of magnitude), resistance to enzymatic degradation, excellent water dispersibility, superior ability to be conjugated to various biomolecules, and versatile to be incorporated into relevant multifunctional theranostic systems [50, 51]. More in general, the photodynamic therapeutic effect of nanostructured metal sulfides either as next-generation PSs is being currently explored for cancer treatment or as photothermal agents to treat other diseases, which will be discussed in detail in the next section.

Metal Sulfides as Photosensitizers in PDT

Among the most studied NMCs in PDT are the metal transition sulfides (MTSs), with a general formula MS_{2-x}, which exhibit unique physical and chemical properties. Depending upon their metal composition, it can crystallize in three main different structures: (i) molybdenite type (MoS_2), (ii) CdI_2-type, and (iii) pyrite (FeS_2). This variability in composition and structure is responsible for MTS nanostructures to have innate physicochemical merits, which have been applied in light emitting devices, photovoltaic devices, catalysts, sensors, and more recently, in theranostics [52]. As for theranostic applications, they have promising advantages to be used as bio-imaging probes, drug delivery cargos, and phototherapy agents due primarily to their strong absorption

in the NIR region (around 700–1100 nm), high extinction coefficients, versatile surface chemistry, high fluorescence, magnetism, structural, and thermal stability, which has boomed significant research in the field of MTSs. Moreover, MTSs are easily obtained through low-cost synthetic methods compared to other NIR absorbing metal NPs, such as gold, silver, and copper [52]. For instance, the cost of 1 mol of Au atoms is estimated to be around $52,200, while the same amount of 1 mol of CuS molecules costs nearly $330 [50]. We highlight below the use of the main types of MTSs as passive and active photosensitizer agents recently published in the literature.

Molybdenum Disulfide

Molybdenum is a transition metal with electronic configuration [Kr] $4d^5$ $5s^1$ and exhibits superior catalytic reactivity because of its half-filled *d* and *s* orbitals. Molybdenum disulfide (MoS_2) part of the transition metal dichalcogenide families are generally prepared by incorporation of Mo sheets into sulfur sheets, which are kept together by intense covalent interactions. MoS_2 nanosheets are atomically-thin two-dimensional (2D) layers analog to graphene that have shown great potential in a wide range of fields, including biomedicine given their unique optical, electronic, and mechanical properties. Reports show that nanostructured MoS_2 could interpenetrate cells via endosomal cell uptake and pinocytosis [53]. In terms of NIR absorbance, Chou et al. first demonstrated that single-layer MoS_2 sheets have higher absorbance in the NIR region than graphene and better extinction coefficient compared to gold nanorods. This study substantially prompted extensive research thereof as NIR-triggered drug delivery platforms and photothermal agents [54]. In PDT, MoS_2 nanosheets have been mostly used as a passive platform due to their extraordinary surface-area-to-mass ratio 2D structure that enables them to load therapeutic molecules more efficiently. In addition, their innate photothermal properties endow these therapeutic platforms with intriguing synergistic effects suitable for cancer treatment. Liu and co-workers were the first to report one of these platforms that consist of lipoic acid-terminated polyethylene glycol (LA-PEG) MoS_2 nanosheets loaded with PS chlorin e6 (Ce6) [55]. They observed a higher cellular uptake of Ce6 upon light irradiation of 800 nm and a significant enhancement in PDT efficiency *in vitro*. This enhancement was ascribed to a mild hyperthermia effect that increases membrane permeability and in turn promotes higher cellular uptake. The photothermally enhanced PDT synergistic effect was similarly demonstrated *in vivo* inducing controlled delays in 4T1 tumor growth in injected mice. A comparable system was reported by Jia and co-workers working with Ce6 labeled with an ATP aptamer before being loaded to MoS_2 nanoplates, which produced a desired drug delivery response [56]. Their studies indicate that after nanoprobe internalization ATP-abundant lysosomes induced the release of the single-stranded aptamer from MoS_2. Subsequently, the Ce6 fluorescence (excitation wavelength 633 nm) allowed the imaging of intracellular ATP and generation of $^1O_2$. This turn-off nanoprobe system reduced the dark toxicity associated to Ce6 and showed enhanced anticancer properties.

Nanostructured MoS_2 has been also regarded as a potent alternative to graphene due to its 2D structural similarity, excellent charge-density wave transition, conductivity, biocompatibility, and superb electrical properties. Recently, for instance, Liu et al. have shown that nanostructured MoS_2 was less hepatotoxic in comparison with graphene oxide [57]. Compared to graphene oxide, nanostructured MoS_2 has a wide range of appropriate properties for applications in energy storage, catalysts, and biomedicines because of their low-cost, exotic features, and physicochemical characteristics [58–60]. Specifically, the great biocompatibility, extremely effective valency, and high sensitivity of nanostructured MoS_2 are more promising than graphene oxide to expand and design nanoprobes for optical imaging, drug delivery, medical bioimaging, and foremost for cancer phototherapy [54, 56, 61]. A "four-in-one" nanoplatform, for instance, based on bioconjugated MoS_2 was constructed and designed by Song et al. to discover favorable imaging-guided phototherapy, photothermal therapy (PTT), and PDT, where the nanostructures were synthesized via the hydrothermal method [61]. The group proposed that nanostructured MoS_2 can be used as a PS material for PDT in cancer treatment (see Fig. 4). In this study, the authors intermixed bovine serum albumin (BSA) with MoS_2 to modify biocompatibility responses and then conjugated with Cy5.5 (a bright, near-IR fluorescent dye) to obtain innovative fluorescence imaging features, as shown in Fig. 4. Through in vitro and in vivo experiments, the nanoplatform was proved to induce photoablation of tumor cells and tissues (see Fig. 4). B-ultrasonography and MR imaging were used to monitor the solid tumor removal after therapy, which showed a liquefaction necrosis process for rehabilitation.

In a separate account, a multifunctional PC10A/DOX/MoS_2 hydrogel system was prepared by Jin *et.al* for chemotherapy/PTT/PDT of 4T1 tumors [62]. The authors also investigated the immune responses caused by the photothermal and photodynamic effect of MoS_2 nanosheet in the hydrogel. PC10A/DOX/MoS_2 were produced by loading positively charged DOX (drug) and negatively charged PC10A (hydrogel) on the surface of MoS_2 nanosheets through a layer-by-layer approach, which resulted to be injectable and possess great

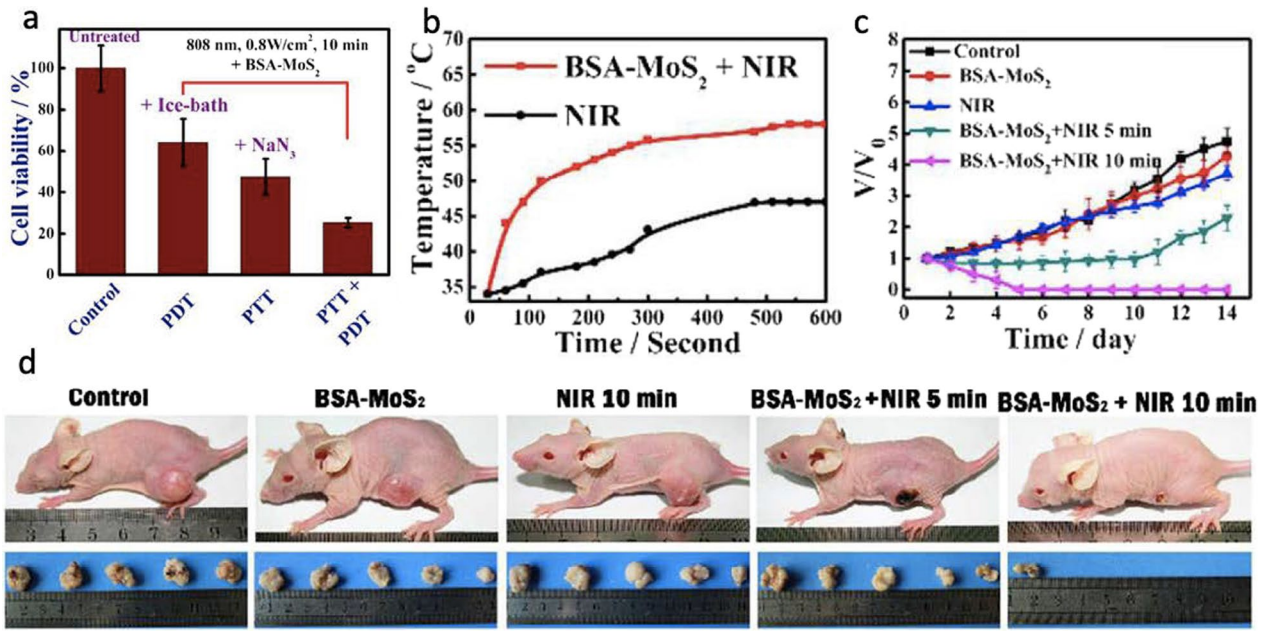

Fig. 4 Relative cell viability of HepG2 exposed to with BSA-MonS_2 after different treatments, including untreated group, only PDT group, only PTT group and PD/PT combined group. **b** Temperature profiles of tumor-bearing m**a**ice under NIR irradiation (with PBS or BSA-MoS2 injection); **c** Relative tumor volume of mice. **d** Representative photographs of mice and tumors. Reproduced with permission from Ref. [61]. Copyright 2017, Royal Society of Chemistry, Washington, DC

biocompatibility. Two-dimensional MoS_2 nanosheets in the hydrogel were then tested as photodynamic agents controlling ROS production. The results indicate that PC10A/DOX/MoS_2 hydrogel in presence of laser exposure can have antitumor immune influences to prevent the development of primal 4T1 breast tumors and distal lung metastatic nodules. The overall findings proved that PC10A/DOX/MoS_2 hydrogel is beneficial for antitumor immunity therapy to treat malignant tumors via PDT. Similarly, Xu et al. (2017) IR-808 dye sensitized upconversion nanoparticles (UCNPs) with a chlorin e6 (Ce6)-functionalized silica layer, which was then integrated with MoS_2 nanosheets for imaging-guided PDT [63]. In this study, MoS_2 nanosheets were synthesized through liquid exfoliation of bulk MoS_2 flakes, which were prepared by molten salt electrolysis method. The nanoplatform shows both abundant ROS and local hyperthermia when exposed to a single 808 nm laser irradiation on the photosensitizer. These in vitro and in vivo tests suggest that this nanoplatform offers great cell killing and tumor inhibition efficacy when both PTT and PDT approaches are combined.

It is noteworthy that some Cd-free NMCs (e.g., molybdenum diselenide, $MoSe_2$) can be also considered as innovative PTT agents with therapy efficacies comparable to MoS_2. $MoSe_2$ exhibits a direct band gap of ~1.5 eV (compared with MoS_2 ~1.8 eV) and excellent long-wavelength NIR absorption, which can induce stronger penetrability in deep-tissue photothermal therapy [64]. A nanosystem of indocyanine green (ICG)-loaded $MoSe_2$ nanoparticles ($MoSe_2$@ICG-PDA-HA) with dual photothermal/photodynamic functions under near-infrared irradiation was developed by Liu et al. [64]. They reported that $MoSe_2$@ICG-PDA-HA can contribute to the production of ROS after a minute exposure of 4T1 tumor cells without affecting D-α-tocopherol succinate-treated groups with free ICG or prior $MoSe_2$ NPs. The authors further found that ICG and $MoSe_2$@ICG-PDA-HA could produce ROS during irradiating with 808 nm NIR laser, which decreased the extra anti-ROS factor (tocopherol). To explore the inhibitory effect of $MoSe_2$@ICG-PDA-HA, the authors incubated the multicellular spheres with PBS, ICG, $MoSe_2$ NPs, and $MoSe_2$@ICG-PDA-HA about 24 h, respectively, and then irradiated 5 min by laser (0.5 W cm^{-2}). The $MoSe_2$@ICG-PDA-HA + Laser group showed the best inhibitory effect on multicellular spheres growth, and the cell sphere volume became the original 41.8%, which was better than the MoSe2 NPs + Laser group (66.7%) and the ICG + Laser group (62.2%). This nanoplatform is a promising system that could enhance the photothermal/photodynamic synergy effect to effectively treat cancer.

Zinc Sulfide

Another type of MTSs used to increase the efficiency of PSs in PDT is zinc sulfide (ZnS), which is a II–VI semiconductor compound that has various applications in nanomedicine [65]. Nanocomposite of reduced graphene oxide (rGO) and $CuInS_2$/ZnS nanocrystals ($CuInS_2$/ZnS/liposome-rGO NCs) was developed to investigate both PDT and PTT. In vivo studies in mice bearing tumors induced by esophageal cancer Eca-109 cells indicate that $CuInS_2$/ZnS/liposome-rGO markedly reduced the tumor size, while in vitro studies revealed a significant induction of apoptosis in human esophagus carcinoma cells upon irradiation of 671-nm laser. The findings show that the nanocomposites not only can produce ROS in the presence of light (671-nm laser), but also turn light into heat energy. In addition, ROS and heat produced by $CuInS_2$/ZnS/liposome-rGO were superior to those produced by $CuInS_2$/ZnS/liposome and rGO nanosheets alone [66].

To understand more the role and capability of ZnS to produce ROS, water-soluble Mn-doped ZnS quantum dots (ZnS:Mn QDs) were investigated by Diaz-Diestra et al. and used as potential PSs [67]. The authors selected the RB/DPBF pair system because the photo-oxygenation pathway can generate $^1O_2$ via a Type-II reaction. In this sense, ZnS:Mn can generate excited singlet state oxygen by energy transfer. They found that the quantum yield of $^1O_2$ is 0.62 in buffer and 0.54 in water in the presence of a chemical scavenger and a standard dye when ZnS:Mn QDs were used as PS (532 nm laser). The authors emphasized that dependency of the reaction on dissolved O_2 showed that $^1O_2$ is produced by the QDs during the photosensitization process and there is no oxidation of DPBF in the absence of light source. The findings were in agreement with a chemical trapping energy transfer mechanism and demonstrate the capability of ZnS:Mn QDs not only as PDT PSs but also as luminescent nanoprobes for cancer theranostics. In a similar study, Martynenko et al. demonstrated an enhanced PDT efficacy for the destruction of Ehrlich ascites carcinoma (EAC) cells using Cd-free ZnSe/ZnS quantum dots (QDs) and chlorin e6 complexes (water-soluble QD-Ce6 complex), when irradiated with 405 nm diode laser (power density of 40 mW cm^{-2}) [68]. The enhanced PDT efficacy of the complex was ascribed to the synergistic effect of the QDs on the Ce6 intracomplex photoexcitation energy transfer and on the increased cellular uptake of Ce6. Further investigation shows that in absence of Ce6 using similar ZnS-based QDs photodynamic effects were induced, which were used on pancreatic cancer cells [69]. After treating human pancreatic SW1990 cancer cells with QDs and irradiating with 365 nm light, the authors detected Bcl-2 and caspase-3 via real-time PCR and protein immunoblotting. In addition, cell viability was remarkably less in the presence of exposure or with a longer incubation time and a superior light dose. Ultrastructural variation in SW1990 cells with organelle degeneration and chromatin condensation and aggregation in the vicinity of nucleus were also observed by the authors when the QDs where light exposed. The authors concluded that the QDs can be used as a promising PS to inhibit SW1990 cell proliferation through ROS generation and apoptotic protein expression regulation.

Copper Sulfide

Copper sulfide ($Cu_{2-x}S$) NPs, a p-type semiconductor, have attracted increasing attention in recent years due to their excellent surface plasmonic absorbance in the NIR region, which can be exploited in theranostic applications. This property originates from the free holes of the unoccupied highest energy states of the valence band, which are strongly dependent on the crystal phase of the NPs and in turn on the Cu/S ratio [70]. Some of the most dominant structural phases include $Cu_{31}S_{16}$ (monocyclic phase), Cu_9S_5 and $Cu_{1.8}S$ (cubic phase), Cu_7S_4 and $Cu_{1.75}S$ (orthorhombic phase), $Cu_{58}S_{32}$ and $Cu_{1.81}S$ (triclinic phase), and CuS (hexagonal phase or covellite). It has been reported that more copper deficiency in the lattice structures ($Cu_{2-x}S$ with $x>0$) is a result of the decrease in the Cu/S ratio, which increases the concentration of free carriers and induces the observed localized surface plasmon resonance (LSPR) absorbance in the NIR region [71, 72]. In a similar analysis, when the Cu/S ratio increases, as in Cu_2S (with $x=0$), the few free carriers (holes) decrease and LSPR is not observed. Besides varying compositions, tuning $Cu_{2-x}S$ NPs morphology can also alter their LSPR. However, through the current synthetic approaches, most of the reported morphologies fall within the microsize regime, hindering further biomedical applications [73]. Compared to plasmonic metals including gold NPs (whose free carrier concentration is fixed and consequently, their LSPR can only be tuned by varying the NP morphology and damping parameter), the LSPR of $Cu_{2-x}S$ NPs can be tuned throughout the NIR region upon varying composition and crystal structure [50, 51, 74]. Consequently, the cost of the therapy could be reduced given the abundance of this metal and the easily scalable synthesis of $Cu_{2-x}S$, which makes them promising candidates as translational phototherapeutic agents. For instance, producing 1 mol of $Cu_{2-x}S$ costs around $330 and 1 mol of Au costs $52,200 [48]. Moreover, $Cu_{2-x}S$ is resistant to photobleaching and photodegradation and, due to its tailorable LSPR, it exhibits fine-tune absorption spectrum and large extinction coefficients in the NIR region. Han et al. [51] reported that bovine serum albumin (BSA)–folic acid (FA) functionalized hollow $Cu_{2-x}S$ nanostructures can be used as

drug delivery vehicle to target indocyanine green (ICG, a NIR-absorbing phototherapeutic agent) to HeLa cells (see Fig. 5). It was demonstrated that this drug delivery strategy significantly improved the stability and reduced the dark toxicity of free ICG, which tends to aggregate in biological fluids. Moreover, the hybrid system exhibited a higher photothermal heating effect and capability to generate $^1O_2$ under laser irradiation, when compared to bare nanocarriers. No obvious cell death was observed when treating the cells with CuS–BSA–FA and CuS–BSA–FA/ICG under dark conditions, however after NIR irradiation, cells were destroyed when CuS/ICG-NIR was used (see Fig. 5).

To date, the use of $Cu_{2-x}S$ as PSs in PDT has been significantly expanded. Wang et al. were the first to report that $Cu_{2-x}S$ NPs not only exhibited photothermal effect but also generated concomitantly high ROS levels under NIR laser light irradiation (at 808 nm and 0.6 W cm^{-2}), which induced human melanoma B16 tumor destruction (see Fig. 6) [74]. $Cu_{2-x}S$ NPs were synthesized by a non-injection approach and capped with oleylamine. The average core diameter was 6.5 nm obtained from TEM analysis. To allow NP dispersion in polar solvents (including water and PBS at pH 7.4), oleylamine was exchanged with amphiphilic thiolated PEG molecules (carboxyl-PEG-SH, molecular weight 3 kDa, and methoxy-PEG-SH, 2 kDa). After the ligand exchange reaction, the authors noticed a blue-shift and intensity increase in the LSPR band ascribed to partial oxidation of the anion sublattice, which introduced additional holes in the upper edge of

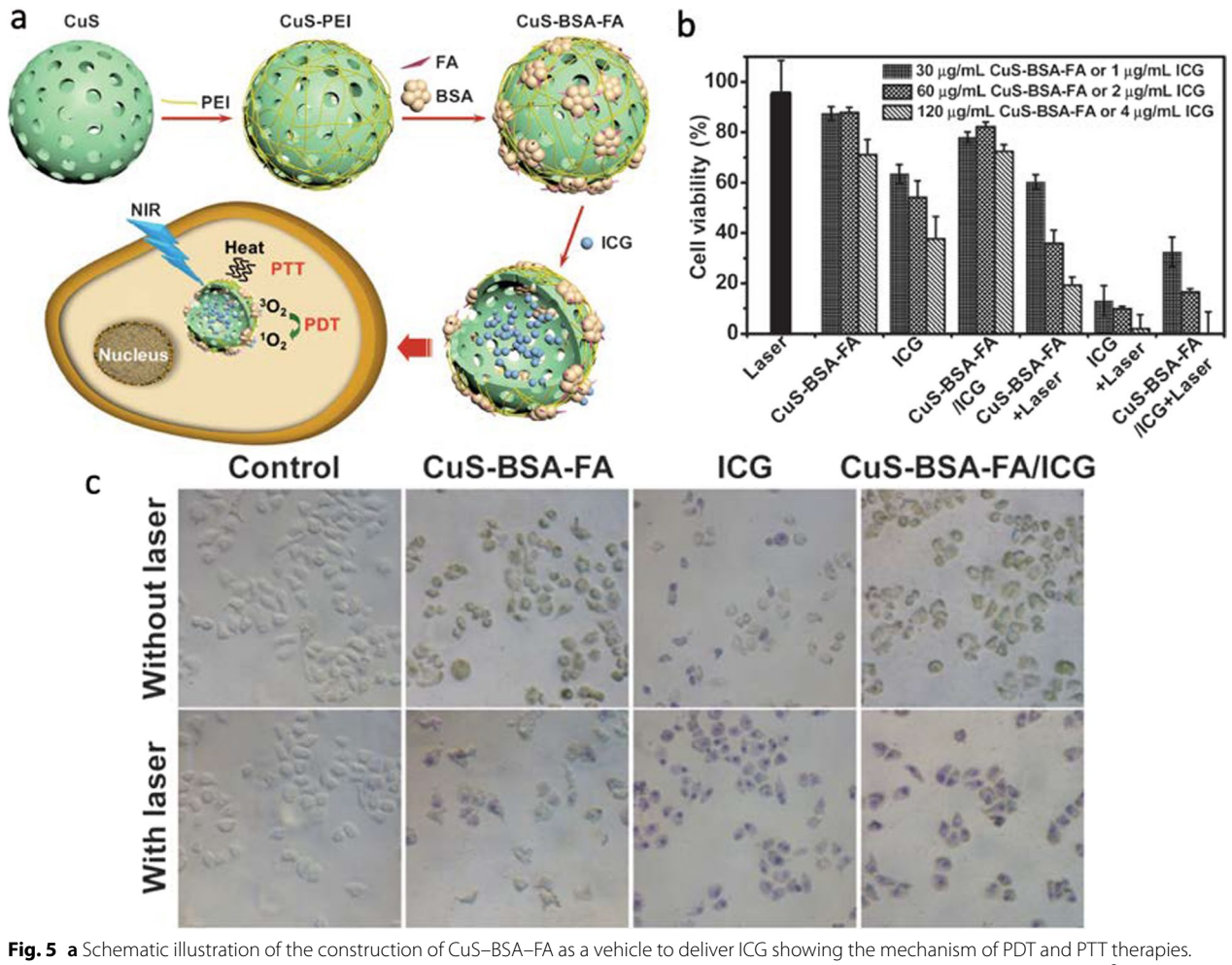

Fig. 5 **a** Schematic illustration of the construction of CuS–BSA–FA as a vehicle to deliver ICG showing the mechanism of PDT and PTT therapies. **b** Cytotoxicity assays on HeLa cells in the presence of CuS–BSA–FA, ICG and CuS–BSA–FA/ICG with or without NIR irradiation (1 W cm^{-2} for 5 min). **c** HeLa cells in the presence of CuS–BSA–FA (60 mg mL^{-1}), ICG (2 mg mL^{-1}) and CuS–BSA–FA/ICG (60 mg mL^{-1} for CuS–BSA–FA and 2 mg mL^{-1} for ICG) with and without laser irradiation (1 W cm^{-2}). Reproduced with permission from Ref.[51]. Copyright 2016, Royal Society of Chemistry, Washington, DC

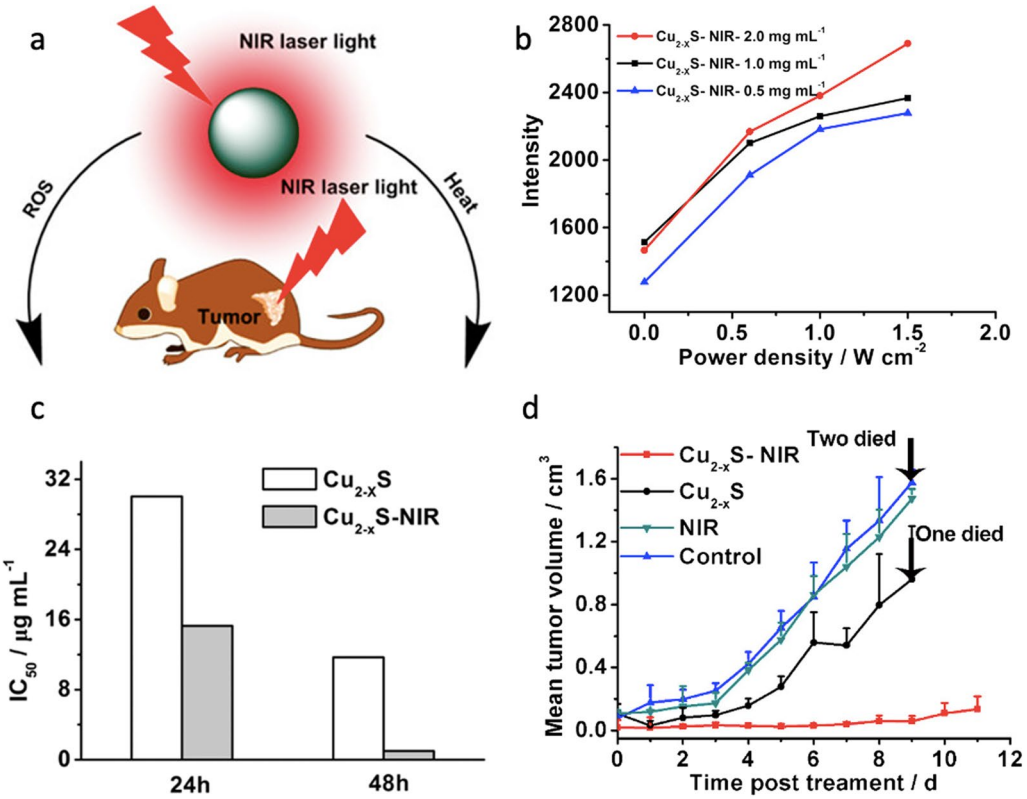

Fig. 6 **a** Illustration showing the near-infrared photothermal and photodynamic therapeutic effect of plasmonic $Cu_{2-x}S$ NCs. **b** The intensity of ESR for the spin trapped hydroxyl radical produced by $Cu_{2-x}S$ NCs at various concentrations and light power densities. Viability of B16 cells at different concentrations of $Cu_{2-x}S$ NCs with and without NIR irradiation (808 nm, 2.3 W cm^{-2} for 3 min) measured after 24 and 48 h incubation. **c** Corresponding IC50 value of each group for 24 and 48 h. **d** Comparative efficacy study of single intratumoral injection in B16 xenograft bearing nude mouse models showing the mean tumor volumes for the $Cu_{2-x}S$-NIR group. Reproduced with permission from Ref. [74]. Copyright 2015, American Chemical Society, Washington, DC

the valence band and consequently a shift in the LSPR to higher energies. The hydrodynamic size of $Cu_{2-x}S$ in PBS was approximately 12 nm, which could allow the NPs to easily extravasate and reach targeted tumor sites.

In the same study, the authors noted that an increase in power density (up to 2.3 W cm^{-2}) resulted in a temperature increase (30.6 °C) of PEG–CuS solution within 10 min, yielding 16.3% of photothermal efficiency when assessed in PBS. A slight aggregation was observed at temperatures higher than 60 °C in PBS, which was attributed to the striping of PEG ligands without significant effects on the NPs photothermal efficiency. The photothermal conversion efficiency (PTCE) was also tested on human melanoma B16 tumor-bearing Balb/c nude mice. The NPs were intratumorally injected at a concentration of 15 (mg kg^{-1}) in Cu, and the mice were irradiated with a NIR laser (at 808 nm, 0.6 W cm^{-2}, and a spot size of 2 cm in diameter) for 100 s. Compared to the control group, the group of animals that received the NPs injection (also exposed to the laser treatment) showed a remarkable temperature increase by approximately 14 °C in the IR thermal map of the tumor region, which was enough to kill the tumor cells in xenografts (see Fig. 6). To shed more light upon the death mechanism pathway, the expression of HSP70, a biomarker for elevated stresses (i.e., elevated temperature), and ROS were measured. A high overexpression of HSP70 led the authors to further investigate the photodynamic properties of the NPs. The methods used to detect ROS were electron paramagnetic resonance (EPR) spectroscopy and a fluorescence assay. The former assay enables the detection of free radicals, such as $^{\bullet}OH$ and superoxide ($^{\bullet}O_2^-$). These radicals form an adduct composed of 5,5-dimethyl-1-pyrroline-N-oxide (DMPO) and 2,2,6,6-tetramethylpiperidine (TEMP) with a spin-trapping agent, which shows typical triplet and quadruple ESR signals. NP solutions at different concentrations (from 0.5 to 2 mg mL^{-1}) were irradiated with NIR light irradiation (808 nm, 0.6 W cm^{-2} for 5 min) and the spectra were recorded. The resulting ESR spectra show the characteristic multiplicity 1:2:2:1

of DMPO-OH and a notorious enhancement of up to 83.5% in •OH levels. No obvious ESR signal was detected for $^1O_2$-spin trapped adducts. Also, the ROS generation induced by NIR light irradiation of $Cu_{2-x}S$ NCs was found to be both concentration and laser power dependent (Fig. 6). The second assay focused on ROS detection monitored the oxidation of non-fluorescent dye dichlorofluorescein diacetate (DCFHDA), which after exposure to ROS was converted to 2,7-dichlorofluorescein (DCF, a highly fluorescent derivative at 529 nm when excited to 495 nm). The assessments were done in cells and aqueous solutions. Under both circumstances, a much higher DCF fluorescence signal was found in $Cu_{2-x}S$ NIR-irradiated samples compared to the controls (neither NCs nor NIR), and only negligible DCF fluorescence was observed in $Cu_{2-x}S$ group (no NIR exposure). An increase in temperature was recorded not only as the NPs concentration increased but also as copper leakage took place. The detected absorbance is ascribed to ROS formation while the emission signals are caused by the cleavage of the acetate groups.

This leakage was proposed as the initiator behind ROS production. Under NIR light and tumor acidic environment, Cu(I) ions leaking from the NCs react with surrounding hydrogen peroxide to form Cu(II), hydroxide, and hydroxyl radicals similar to that produced in a Haber–Weiss reaction. This ROS production along with the increase in temperature leads to tumor cell destruction. The combination of both therapies enhanced the in vitro and in vivo therapy results. In the in vitro tests, B16 cells were treated with PEG-$Cu_{2x}S$ NPs, and exposed for 3 min to an 808 nm NIR laser with a power density of 2.3 W cm^{-2}. All the experiments evidenced increasing cytotoxicity against B16 cells in a dose and time-dependent manner. After 48 h, the IC50 values (0.995 μg mL^{-1} Cu) for $Cu_{2-x}S$ -NIR were about 11 times lower compared to those obtained at 24 h for the exposed group (15.27 μg mL^{-1}). Fluorescence microscopy revealed disruption of the cell cytoskeleton for the treated group, while the control group treatments did not cause any significant disruption. The therapeutic efficiency was further assessed in vivo in B16 subcutaneous tumor-bearing nude mice for the $Cu_{2-x}S$-NIR treated group and an inhibition of 90% was observed compared to the control group. The therapeutic efficiency is ascribed to the combination of PTT and PDT, making $Cu_{2-x}S$ promising for cancer treatment. Wang's findings have catalyzed the development of other dual PDT and PPT $Cu_{2-x}S$ agents and paved the way for research on the mechanism behind intracellular ROS production. In this spirit, Li et al. prepared 5-nm pegylated $Cu_{2-x}S$ NPs and studied their photothermal and photodynamic activities for the treatment of lung adenocarcinoma SPC-A-1 in vitro and in vivo. SPC-A-1 lung cancer cells incubated with PEG-$Cu_{2-x}S$ NPs were irradiated with an 808-nm laser (1 W cm^{-2} power density). The in vitro combined therapy caused approximately 70% reduction in cell viability, whereas in the control cells incubated with $Cu_{2-x}S$ NPs without laser irradiation, no decrease in cell viability was observed. In the in vivo combined therapy, the mice bearing SPC-A-1 tumors were injected with PEG-$Cu_{2-x}S$ NPs, followed by irradiation using an 808-nm laser, and the tumor volume was monitored for 2 weeks. Tumor suppression and delay in growth were observed for the mice group treated with NIR and PEG-$Cu_{2-x}S$ NPs under irradiation, which was ascribed to the synergistic effect of NPs. Tumor tissues were collected and histochemically stained with hematoxylin and eosin. For the treated group, nuclear pyknosis, cytoplasmic edema, and some leaking patches of eosinophils were observed in the tissues, which are indicative of tumor necrosis. A decrease in the expression of Ki-67, a nuclear non-histone protein frequently overexpressed in proliferating cells, further confirmed the effectiveness of the dual therapy. Through a fluorescent assay, $^1O_2$ was ascertained as one of the ROSs produced for IR-activated $Cu_{2-x}S$ in tumor cells.

To further improve the PTCE and ROS generation of $Cu_{2-x}S$ NPs, hollow-structured $Cu_{2-x}S$ nanocubes were developed following a Kirdenkall approach [75]. CuO nanocube and thioacetamide were used as precursor and sulfur source, respectively, under optimized reaction time and reagent concentrations. The particle size ranges from 250 to 300 nm. Given their hollow structure, $Cu_{2-x}S$ nanocubes (compared to spherical 100 nm $Cu_{2-x}S$ NPs) showed improved PTCE (30.3%) and good structural stability against laser exposure. This enhancement was related to the enhanced light reflex observed in hollow structures (mirror cavity effect). Moreover, given the porous cavity of the $Cu_{2-x}S$ hollow structure and the negative surface potential, doxorubicin, an anticancer drug, was loaded and showed a significant loading capacity of 15.49%. The in vitro synergistic effect of the chemotherapy associated to PTT and PDT displays enhanced cytotoxicity on HepG2 cancer cells, as shown in Fig. 7. ROS generation was assessed in vitro and in PBS via the DCFH-DA assay. Strong green fluorescence was observed for cells treated with NIR-$Cu_{2-x}S$ NPs. To detect the possible active ROSs, the author added two scavengers (p-benzoquinone and isopropanol) to the DCFH-DA PBS solutions. The addition of these scavengers induced a decrease in fluorescence signal, suggesting the formation of ·OH and $\cdot O_{2-}$ radicals.

The authors also measured the fluorescence spectra of DCFH treated with Cu^+, Cu^+ (ethanediamine, a chelating agent of Cu ion), Cu^+ (N_2 bubble), and Cu^{2+} solution to further confirm the effect of Cu^+ ions on ROS

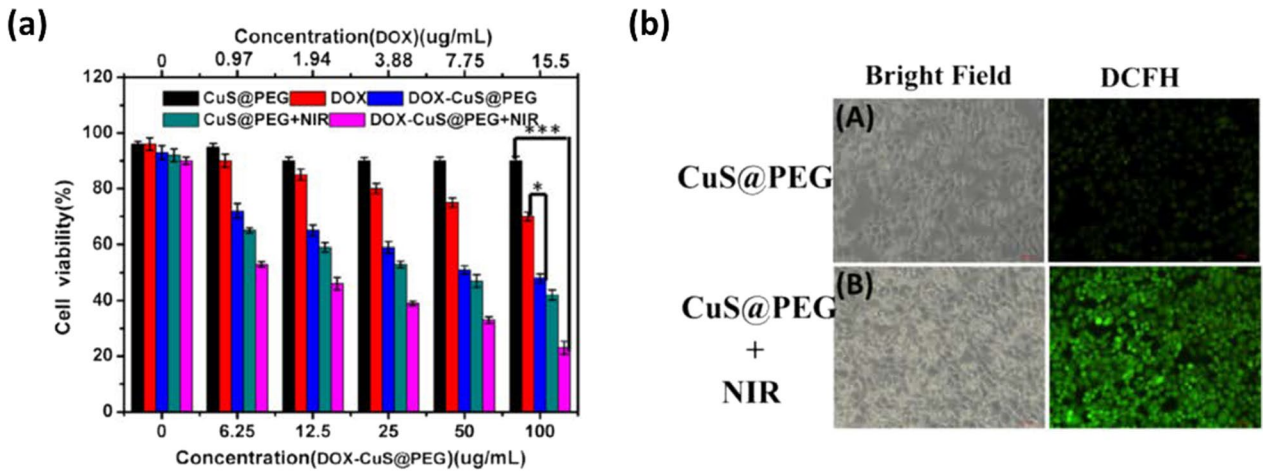

Fig. 7 **a** Cell viability of HepG2 cells incubated with DOX-CuS@PEG nanocubes at different concentrations and subjected to NIR laser exposure (808 nm, 2 W cm^{-2}) for 20 min. **b** Fluorescent images of DCFH stained HepG2 cells after curing with C_US@PEG with and without exposure of 808 nm light (2 W cm^{-2}) for 10 min. Reproduced with permission from Ref. [75]. Copyright 2019, Elsevier, Amsterdam, Netherlands

production. Only under the first condition, ROS generation was detected, which further confirmed the pivotal role of Cu^+ in the photodynamic activity of $Cu_{2-x}S$ NPs. In addition, it was noted that an increase in temperature and immersion time considerably benefits the ROS production, which reinforces the PTCE relevance of these NPs. Based on these findings, the proposed mechanism for Cu-based PSs is as follows.

Firstly, Cu^+ leaked from the NPs reacts with the surrounding O_2 (oxidizes to Cu^{2+}) through a single electron process

$$O_2 + Cu^+ \rightarrow Cu^{+2} + O_2^- \quad (1)$$

Then, $\cdot O_2-$ can further react with the surrounding Cu^+ to produce H_2O_2,

$$O_2^- + Cu^+ \rightarrow Cu^{+2} + H_2O_2^- \quad (2)$$

This Cu^{2+} can react with H_2O_2 through the Haber–Weiss and Fenton reactions generating ·OH keeping the cycle between Cu^+ and Cu^{2+} redox states,

$$H_2O_2 + Cu^{2+} \rightarrow Cu^+O_2H + H^+ \quad (3)$$

$$H_2O_2 + Cu^+ \cdot O_2H \rightarrow Cu^+ + O_2 + OH + H_2O \quad (4)$$

Considering the abundant hole carriers in CuS nanomaterials, a second mechanism was proposed for ROS generation, which would be mediated through a reaction between holes and water molecules (photocatalysis). However, some questions remain open regarding the exact ROS production mechanism, which requires further study for the improvement of the therapy.

In pursuit of developing CuS-based systems that exhibit similar synergistic photothermal and photodynamic effect on cancer cells, Huang et al. reported a yolk-shell structure of $Cu_{2-x}S$ and upconversion nanoparticles (UCNPs) [76]. The as-prepared UCNPs@CuS system showed higher generation of ROS species (such as hydroxyl radicals and $^1O_2$) when compared to bare CuS counterparts. The PDT effect combined to an enhanced photothermal effect resulted in significant death of 4T1 murine mammary carcinoma cells under an irradiation of 808 nm. Likewise, Chang et al. developed a yolk-shell nanoparticles (YSNPs) of gold (Au) core@void@copper sulfide (CuS) shell (Au-CuS) for chemo-, photothermal, and photodynamic combination therapy of cancer [77]. The authors observed that this structure facilitates the incident light to be concentrated into nanoscale hotspots of plasmonic metal cores, when there is a match of the incident light wavelength with the LSPR absorption wavelength of the plasmonic metal core, which produces local electromagnetic field enhancement to induce a resonance energy transfer (RET) from the plasmonic metal to the semiconductor. The activation of RET process could be thereby used in plasmonic metal core@void@CuS shell YSNPs for improvement of both photothermal and photodynamic performance of CuS (see Fig. 8), as the authors indicated.

RET activation was proved to significantly improve the photothermal performance to almost 50% compared to their bare counterparts (p-CuS HNPs and Au) and other physical mixtures. RET activation from Au core to CuS shell also enhanced the electron–hole pair in CuS shell, facilitating more radical formation thus resulting in superior photodynamic performance. Interestingly, no other

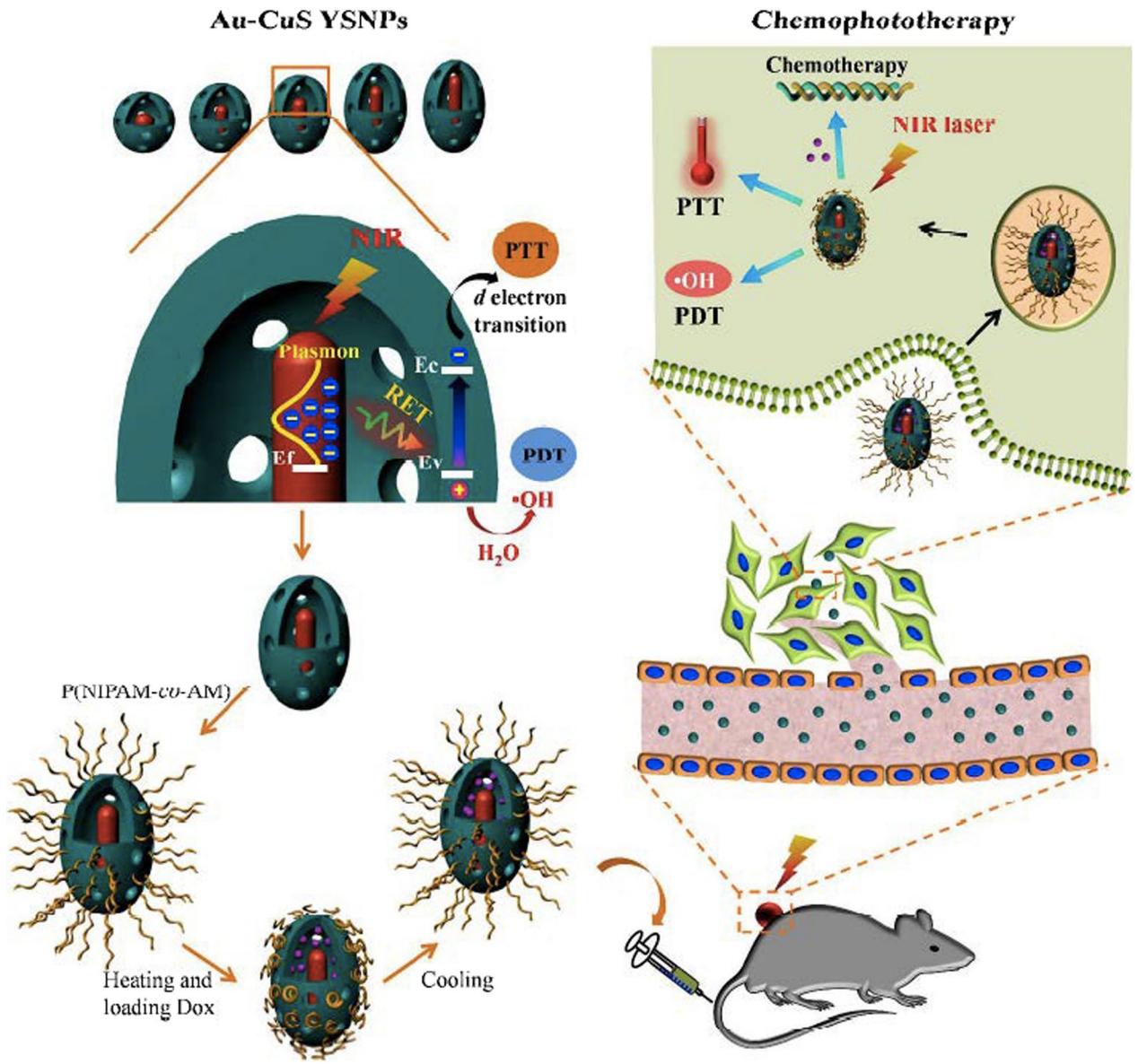

Fig. 8 Graphical representation showing the improved therapeutic performance of Au-CuS YSNPs based on resonance energy transfer (RET) activation that can be used for chemo-, photothermal, and photodynamic combination therapy. Reproduced with permission from Ref. [77]. Copyright 2018, American Chemical Society, Washington, DC

ROS species such as $^1O_2$ and $\cdot O_2^-$ were detected, which could be indicative of a type I PDT process that might be useful for the treatment of hypoxic tumors. To optimize and obtain the most effective RET process of Au-CuS YSNPs, the morphology of Au cores was varied from nanospheres to nanorods yielding different LSPR absorption peaks at 520, 700, 808, 860, and 980 nm. It was found that Au_{808} and Au_{980} induced the highest temperature elevation and ·OH production under 808 and 980 nm laser irradiation, respectively. Similarly, increasing of shell thickness reduced the RET efficiency. Through in vivo studies, the authors concluded claiming that p-Au-CuS YSNPs exhibit efficient tumor accumulation, effective tumor growth inhibition, excellent biocompatibility in 4T1 tumor-bearing mice, and superior photodynamic properties to treat cancer (see Fig. 9).

Other Metal Sulfides

More recently, other nanostructured metal sulfides with unique physical and chemical properties and promising

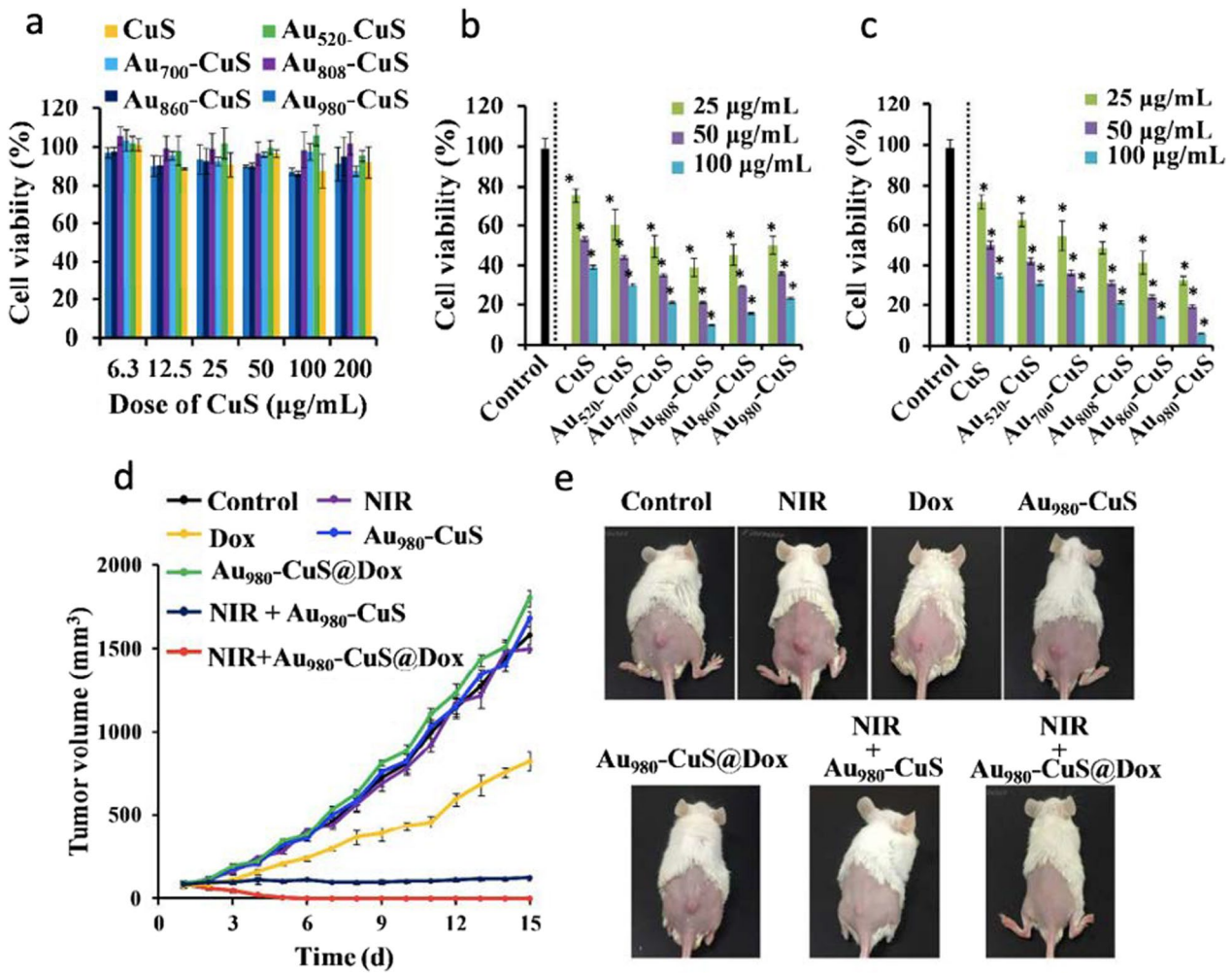

Fig. 9 **a** Viability assessment of 4T1 cells exposed to different concentrations of NPs (CuS content) for 24 h. **b**, **c** Viability assessment of 4T1 cells treated with different concentrations of NPs for 6 h, followed by 5-min irradiation by an 808 nm (**b**) or 980 nm (**c**) laser at 0.75 W cm^{-2} and another 18 h of incubation. **d** Tumor growth curves of 4T1 tumor-bearing mice after IV injection with PBS, Dox, p-Au_{980}-CuS, p-Au_{980}-CuS@Dox in the presence (980 nm laser, 0.9 W cm^{-2}, 5 min) and absence of irradiation. **e** Representative photos of tumor-bearing mice after treatment. Reproduced with permission from Ref. [77]. Copyright 2018, American Chemical Society, Washington, DC

photodynamic response for cancer treatment have been reported. Among them, iron sulfide [78], silver sulfide [79, 80], bismuth sulfide [81, 82], and cobalt sulfide [83] stand out. Iron sulfide comprises iron and sulfur at different proportions and exists in different phases, such as $Fe_{1-x}S$ (pyrrhotite), FeS (mackinawite), FeS_{2p} (pyrite), Fe_3S_4 (greigite), Fe_9S_{11} (smythite), and FeS_{2m} (marcasite) [78]. The phase, shape, and physicochemical properties of iron sulfide nanoparticles depend primarily on the iron content [78]. FeS_2 is considered a non-toxic material and its production is cost-effective due to the high abundance of its elements [84]. Its unique magnetic properties, biocompatibility, biodegradability, and facile synthesis, make FeS_2 attractive as a theranostic agent [85, 86]. Inspired by these excellent features, Jin et al. developed a nanodot system based on FeS_2@BSA-Ce6 and evaluated its efficiency on murine breast cancer (4T1) cells (see Fig. 10) [87]. The authors found that FeS_2@BSA-Ce6 nanodots induce significant cell death and slow tumor growth upon irradiation (660 nm xenon lamp at 5 mW cm^{-2} for 30 min), as shown in Fig. 10. Also, in efforts to merge PDT and PTT therapies using FeS_2, Li et al. investigated the efficiency of FeS_2@C-PEG yolk-shell nanostructures in both therapies [88]. They reported that both the particles excited by the light source and dissolved O_2 played critical roles in producing ROS. The authors also conjugated the indocyanine green (ICG) photosensitizer to FeS_2@C-PEG to enhance the PDT and PTT efficiency.

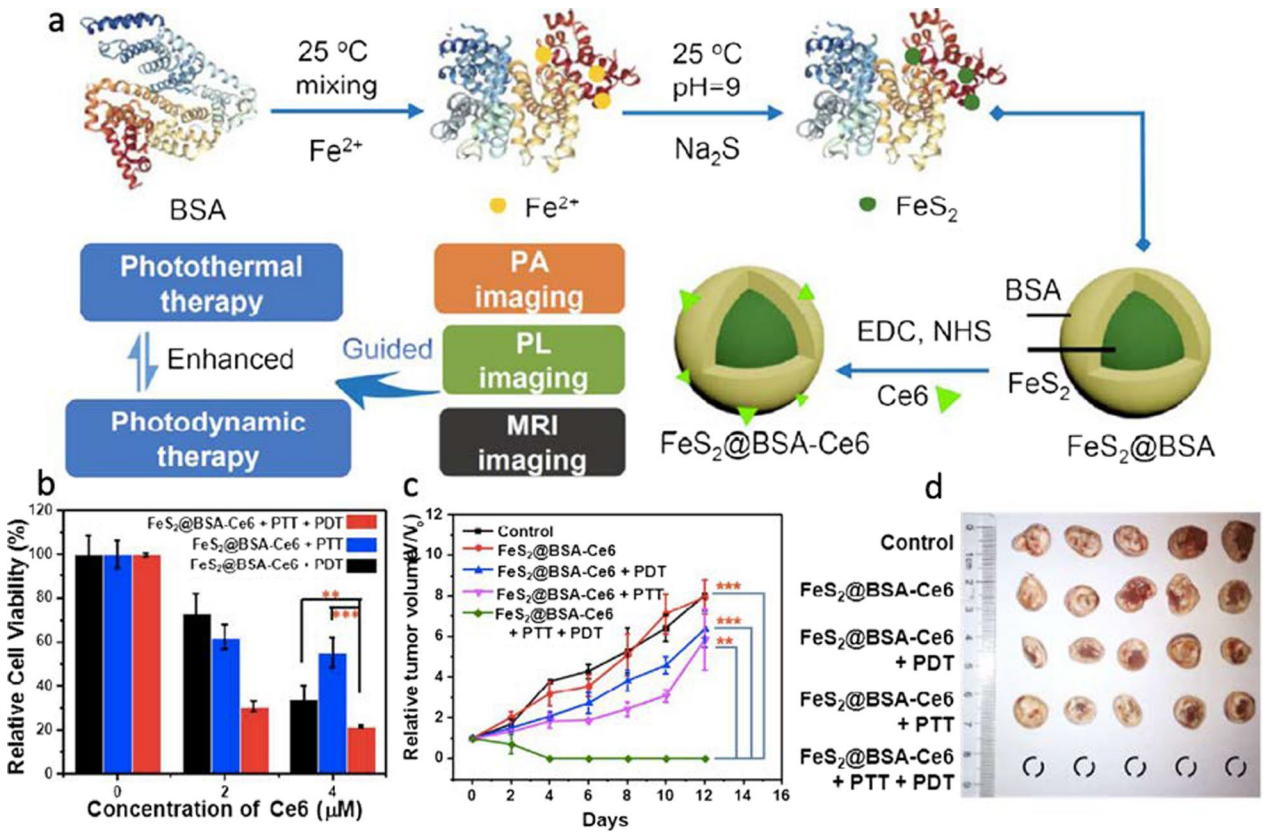

Fig. 10 **a** Synthetic route and photodynamic effect of FeS_2@BSA-Ce6 for PDT and PTT therapies. **b** Cells treated with FeS_2@BSA-Ce6 and irradiated by a 660-nm lamp (5 mW cm^{-2}, 30 min), 808-nm laser (0.8 W cm^{-2}, 20 min) or both. **c** Relative tumor volume curves and corresponding **d** photograph of tumors collected from different groups (PBS-control, FeS_2@BSA-Ce6, FeS_2@BSA-Ce6 + PDT, FeS_2@BSA-Ce6 + PTT, and FeS_2@BSA-Ce6 + PTT + PDT). Reproduced with permission from Ref. [87]. Copyright 2018, American Chemical Society, Washington, DC

It was observed that FeS_2@C-PEG can oxidize water to form O_2 under NIR exposure, which can in turn increase the therapy efficiency. Furthermore, the authors claimed that the Fenton reaction of Fe(II) makes FeS_2 degrade intracellular H_2O_2 to produce more effectively ·OH and O_2.

Another interesting nanostructured metal sulfide system is silver sulfide (Ag_2S) that exhibits excellent biocompatibility, superior optical properties, and a wide range of applications, including bioimaging, fluorescent detection of molecules and metal ions, electronics, catalysis, and energy conversion. Recently, Ag_2S NPs have been proposed to serve as PSs for PDT to treat more aggressive, chemoresistant and non-solid tumors. For instance, Wang et al. reported the synthesis of Ag_2S NPs using bovine serum albumin (BSA) as a stabilizer to treat lymphoma [89]. In vitro studies confirmed that Ag_2S NPs could significantly control the proliferation of human lymphoma cells compared to hepatoma carcinoma cells under light irradiation (see Fig. 11). The authors used a diode laser with a wavelength ranging from 400 to 600 nm (power of 0.4 W cm^{-2}) to irradiate the samples for 10 h. They noticed that the strongest absorption peak occurred in the range of 200–600 nm indicative of the strong photoabsorption response of Ag_2S NPs. Finally, Ag_2S NPs can also induce both ROS accumulation in human lymphoma cells under light irradiation and significant disruption of energy metabolism (see Fig. 11). In a separate account, Cheng et al. reported the photodynamic therapy of Ag_2S QDs and its enhanced regulation based on polydopamine (PDA) to treat mammary carcinoma (see Fig. 12) [90]. The authors modified the surface of Ag_2S QDs with PEGylated phospholipids (DSPE-PEG_{2000}-NH_2) to generate $^1O_2$ under irradiation of 808-nm NIR light. To further increase ROS production, Ag_2S QDs were coupled with PDA (PDA-Ag_2S) resulting in significant enhancement of PDT effect. In vitro studies showed identical PDT effects of Ag_2S and PDA-Ag_2S at longer wavelength under irradiation of 660 nm nm laser. Whereas in vivo therapeutic assays on 4T1 tumor bearing female mice revealed that PDA-Ag_2S showed an improved PDT efficacy when compared to Ag_2S (see Fig. 12). This new PS with longer

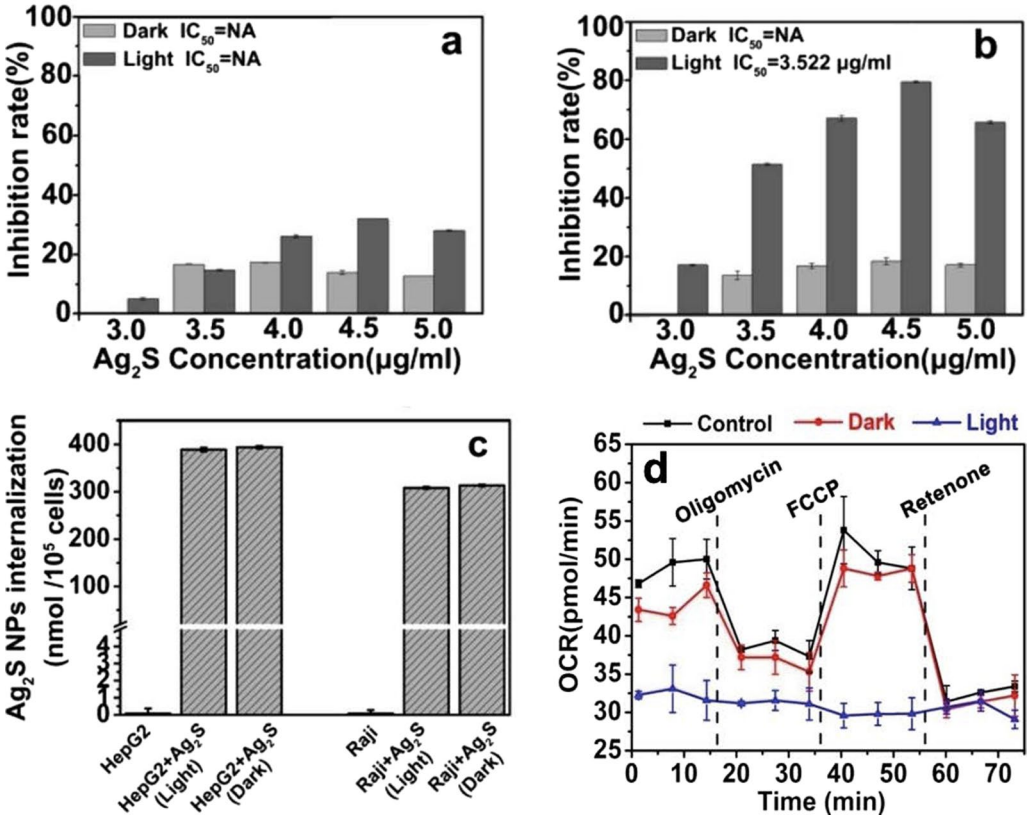

Fig. 11 **a** Proliferative effects of **a** Hep G2 cells and **b** Raji cells treated with Ag_2S NPs under dark and light irradiation for 72 h. **c** ICP-MS analysis showing Ag_2S NP amounts internalized in Hep G2 and Raji cells under dark or light irradiation. **d** Cellular oxygen consumption rate (OCR) of Raji cells by treatment with Ag_2S NPs under dark and light irradiation. Reproduced with permission from Ref. [89]. Copyright 2019, Royal Society of Chemistry, Washington, DC

absorption wavelength (deeper tissue penetration) and enhanced regulatory effect originated from PDA has enormous advantages to expand the application of PDT in tumor therapy.

In parallel, similar nanostructured metal sulfide systems have been reported to treat other types of cancer via PDT and PTT. In this regard, Faghfoori et al. developed a nanosystem based on bovine serum albumin-coated Bi_2S_3 (Bi_2S_3@BSA) NPs conjugated with methotrexate (MTX) to form Bi_2S_3@BSA-MTX NPs to study its anticancer effect on human colon adenocarcinoma [91]. *In vitro* chemo-radiation therapy findings revealed that the viability of treated cells with Bi_2S_3@BSA-MTX NPs is significantly lower than the cells treated with Bi_2S_3@BSA NPs. The apoptosis assay, without X-ray radiation, showed that Bi_2S_3@BSA-MTX NPs (at 300 μg mL^{-1}) induced a significant percentage of cell death while Bi_2S_3@BSA-MTX NPs (at 100 μg mL^{-1}), with X-ray irradiation, demonstrated a considerable rate of apoptosis, which confirmed the ability of the Bi_2S_3@BSA-MTX NPs as radio-sensitizer and their potential therapeutic efficacy in living organisms. To treat other types of cancer, Cheng et al. studied the computed tomography (CT) imaging-guided photodynamic and photothermal properties of bismuth sulfide (Bi_2S_3) nanorods (NRs) linked to zinc protoporphyrin IX (ZP) (BPZP) through a thermally retractable poly(N-isopropylacrylamide-co-acrylamide) (P(NIPAM-co-AM)) polymer, which were intravenously administrated to 4T1 tumor-bearing mice (see Fig. 13) [92]. The authors observed that the fast electron–hole recombination within low bandgap of Bi_2S_3 significantly precluded the photodynamic response. They also observed that the heat released from Bi_2S_3 NRs upon NIR laser irradiation could retract the polymer and drive ZP to the proximity of Bi_2S_3 NRs, which facilitates an efficient electron–hole separation in ZP and Bi_2S_3 NRs and leads to ROS generation. Mechanistically speaking, the ZP molecules play a crucial role in effectively binding to the active site of the HO-1 enzyme to suppress the cellular antioxidant defense ability, and in fostering the subsequent ROS injury in absence of IR irradiation. Also, such molecules can promote efficient electron–hole

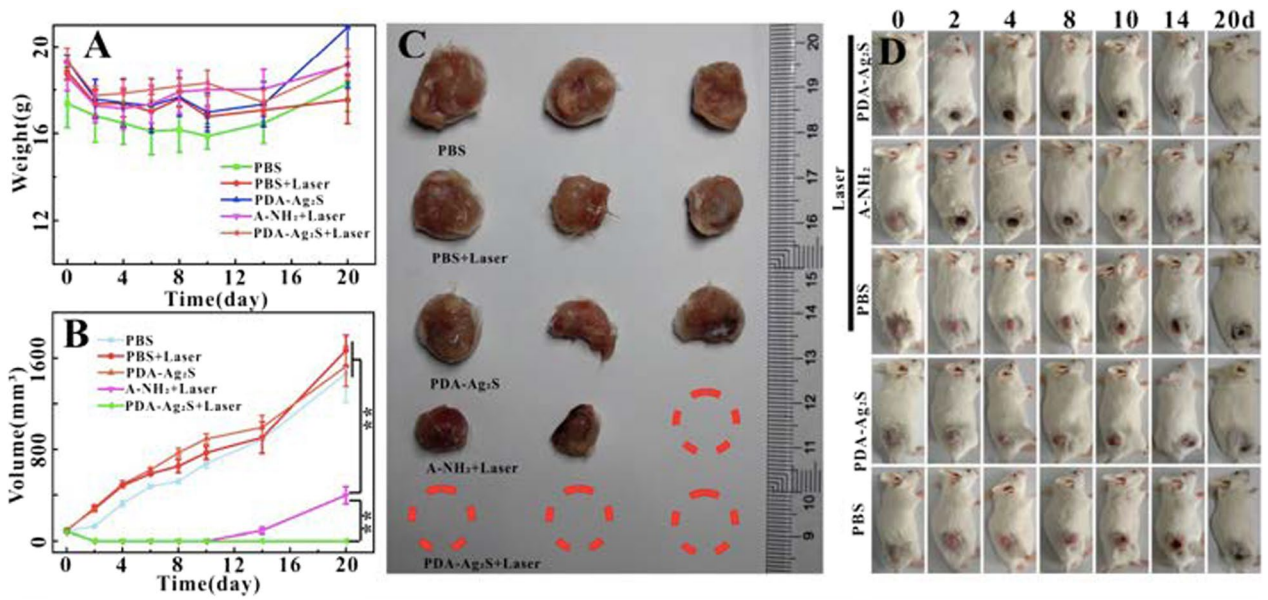

Fig. 12 Tumor weight (**A**) and volume (**B**) change, tumor white-light (**C**), white light (**D**) after tumor irradiation (10 min, 808 nm, 1 W cm^{-2}) in tumor bearing mice after injection of PBS, A-NH_2 and PDA-Ag_2S. Reproduced with permission from Ref. [90]. Copyright 2019, Chemistry Europe, European Chemical Societies Publishing

separation to enhance ROS generation by transferring NIR laser-induced holes from Bi_2S_3 to ZP. As concluding remarks, the authors stated that BPZP can accumulate into tumor, inhibit tumor HO-1 activity (see Fig. 13), and enhance NIR irradiated oxidative injury. BPZP can act as an effective and biocompatible antitumor nanosystem in PDT and PTT.

The last nanostructured metal sulfide system to mention is cobalt sulfide, which has intrinsic peroxidase-like activity useful in PDT to treat cancer. Cobalt chalcogenides are typically synthesized for NIR light activatable PTT due to their high photothermal conversion efficiency and broad optical absorption in the NIR region [93]. Cobalt sulfide ultrasmall NPs are also applicable for systemic circulation of theranostic agents and used as NIR responsive nanostructures for PTT/PDT therapies. There are however some challenges to synthesize biocompatible cobalt sulfide NPs, which demands to employ innovative surface modification strategies. To address these challenges, Lin et al. synthesized multifunctional cobalt sulfide nanodots (Co_9S_8 NDs) using an albumin-biomineralized approach for photocatalytic synergetic therapy with tumor multimodal imaging navigation (see Fig. 14) [83]. The synthesis was driven by breeding BSA with $CoCl_2$ to form the Co^{2+}-BSA complex in the presence of Na_2S to trigger the nucleation of Co_9S_8 NDs. The authors used 1,3-diphenylisobenzofuran (DPBF) as a probe for $^1O_2$, which can decrease the fluorescence intensity of DPBF due to oxidation reaction. They found that upon NIR irradiation (808 nm, 0.75 W cm^{-2}) the NDs dispersed in aqueous solution at 100 μg mL^{-1} Co showed a marked time-dependent $^1O_2$ production, and the DPBF fluorescence decreased ~ 40% in the presence of NDs. This suggests that the NDs can generate $^1O_2$ when NIR irradiated. Also, NIR irradiation stimulated charge collection and separation at the surface thereby decreasing the recombination of photo-triggered charge carriers and accelerating the surface-dependent reactions, which can enhance the photosensitization of Co_9S_8 NDs. The results showed that Co_9S_8 NDs are photostable with photothermal conversion efficiency of 64%. Then the authors irradiated.

K7M2 cells (808 nm laser) at different power densities after incubation with the NDs (25 μg mL^{-1} Co) for 6 h. It was found that all NDs-treated cells were killed under NIR irradiation at 0.75 W cm^{-2} for 10 min (see Fig. 14). Based on these results, the authors investigated if this effective photocatalytic and photothermal effect can be translated into in vivo settings to treat tumors. To do this, the authors intravenously injected NDs into mice bearing K7M2 tumors, and then tumors were irradiated with 808 nm laser at 24 h post-injection. After 5 min of laser treatment, the surface temperature of tumors on NDs group reached about 60 °C, while less than 5 °C was observed for irradiated tumors on PBS group. After continuously monitoring for 21 days, the authors found that the tumor volume of the other groups showed a three–fivefold increase (compared to their original volume) and

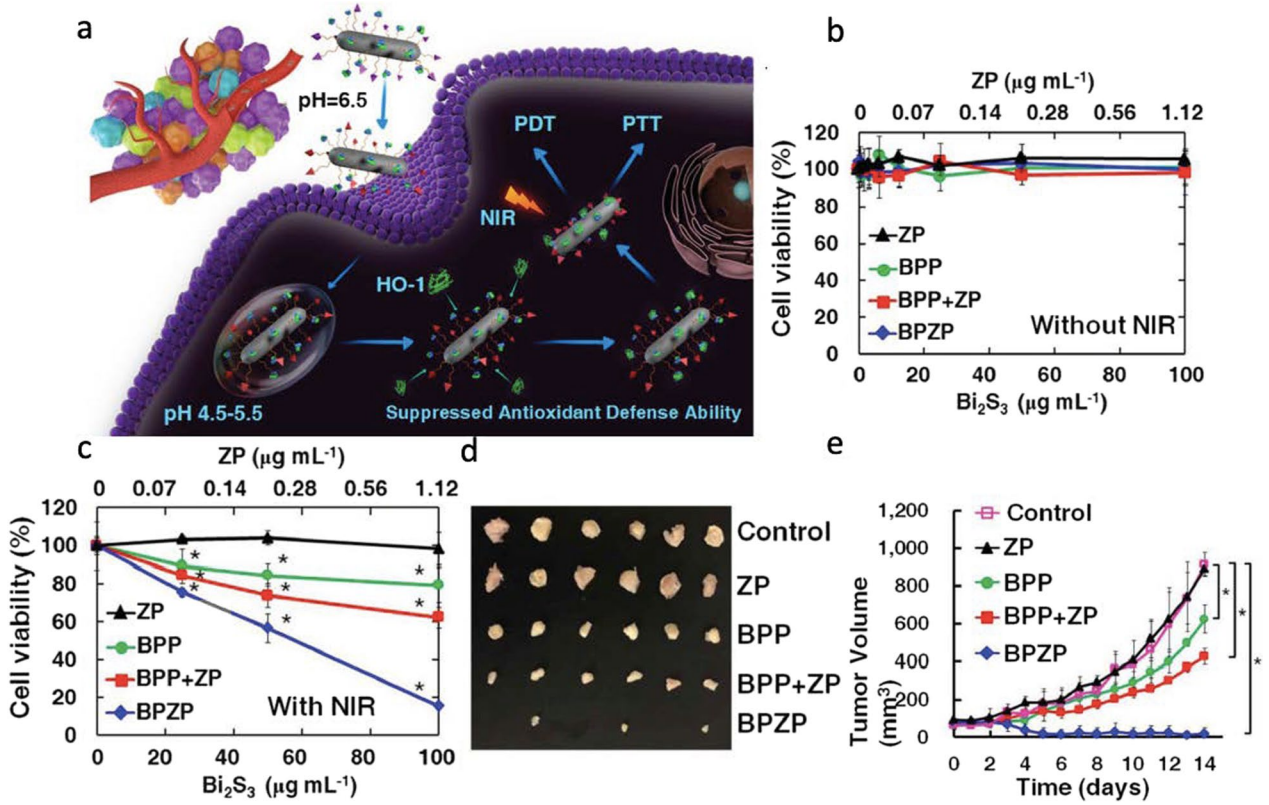

Fig. 13 **a** Schematics illustrating the in vivo therapeutic process using a Bi_2S_3 nanorod-P(NIPAM-co-AM)-zinc protoporphyrin IX-Pep (BPZP) system through suppressing HO-1 activity and promoting NIR laser-irradiated ROS production after intravenous administration. **b**, **c** Viability of cells treated with various concentrations of ZP, BPP, BPP + ZP, and BPZP for 24 h with or without 808 nm laser irradiation (0.75 W cm^{-2}, 10 min). **d** Representative photos of tumors dissected at 14 d post-treatment. **e** Tumor growth curves of mice IV injected with ZP, BPP, BPP + ZP, and BPZP (equivalent to 20 mg kg^{-1} Bi_2S_3 or 0.224 mg kg^{-1} ZP) with 808 nm laser irradiation (0.75 W cm^{-2}, 5 min) for 14 d. Reproduced with permission from Ref. [92]. Copyright 2019, WILEY–VCH Verlag GmbH & Co. KGaA, Weinheim, Germany

only NDs treated group exhibited tumor growth inhibition (see Fig. 14). Co_9S_8 NDs can under NIR irradiation generate ROS to inducing cancer cell death, completely suppressed the tumor growth and even eradicated the tumor. The authors concluded stating that this biomimetic strategy could represent a significant progress for enhanced PTT/PDT synergistic therapy with single NPs under NIR irradiation.

Even though PDT shows certain limitations associated to limited light-penetration depth (for visible light source < 1 mm), MTSs acting as next-generation PSs and phototherapy agents have the potential to address these issues. They possess strong absorption in the NIR region (around 700–1100 nm), high extinction coefficients, and versatile surface chemistry. Biocompatible MTS PSs can also serve as carrier nanoplatforms to address issues related to low solubility, poor tumor selectivity and undesirable pharmacokinetics of traditional PSs. MTS PSs also exhibit promising physicochemical properties, including Fenton catalysis, light conversion, radiation enhancement, and immune activation, and synergistic antitumor properties, which are used in cancer therapy.

Conclusions and Outlook

Over the past decades, PDT has emerged as a promising technique for cancer therapy. Despite its wide application, PDT poses several challenges related to low tissue penetration of excitation light, instrumentation, tissue oxygenation, and inherent photo-biochemical properties of PSs that limit its clinical efficacy. As a result, it is mainly employed for the treatment of superficial tumor or lesion in recent clinical settings. While some studies in PDT attempted to utilize diode laser light and design NIR light-triggered PSs to overcome tissue penetration-based concerns, issues of innate toxicity and hydrophobicity of PSs remain profoundly challenging [94–96].

These challenges are topics of active research, and the advances in nanomedicine have led to brisk progress in the development of sophisticated PSs that promise to overcome such innate biochemical properties to some

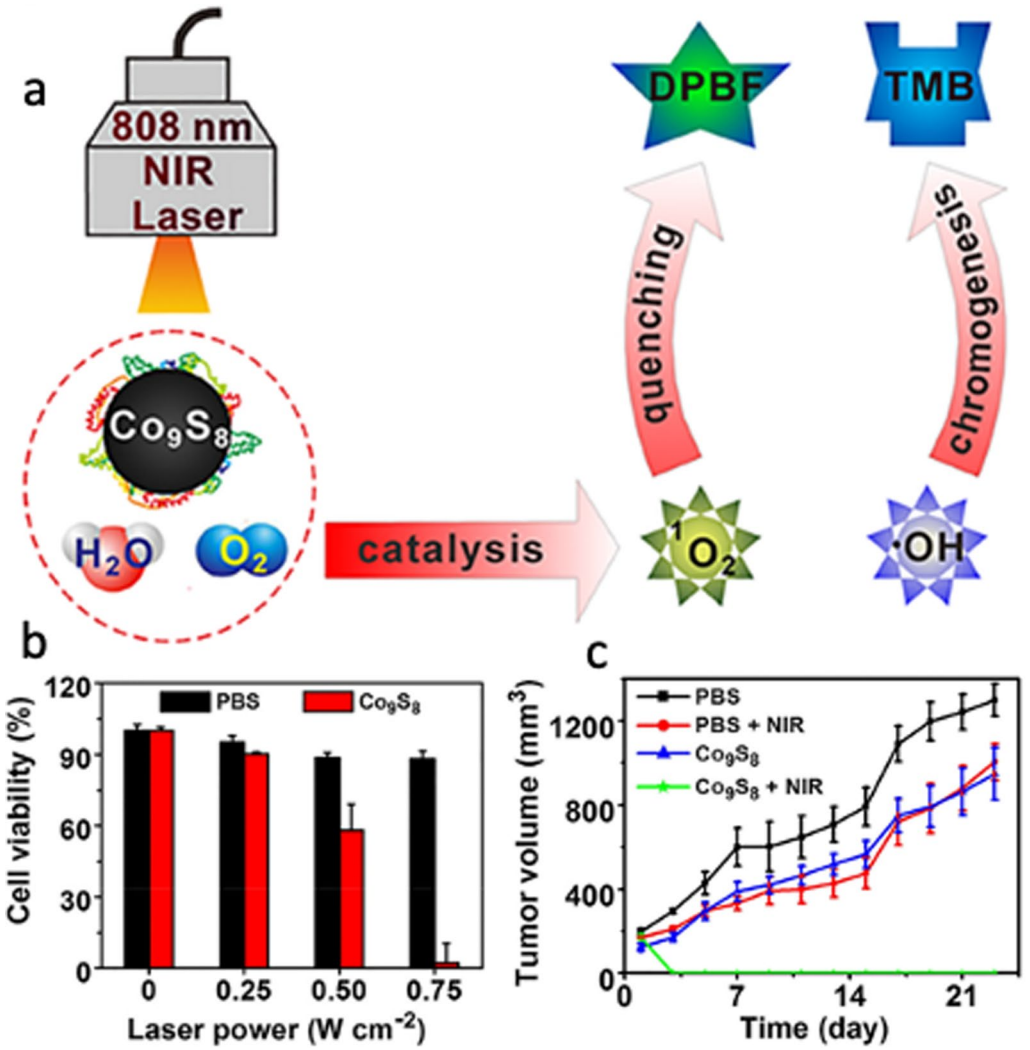

Fig. 14 **a** Schematic illustration of the photocatalytic activity of Co_9S_8 nanodots upon NIR irradiation. **b**, **c** Cell killing and tumor inhibition capabilities of Co_9S_8 nanodots in PDT and PTT therapies. Reproduced with permission from Ref. [83]. Copyright 2018, American Chemical Society, Washington, DC

extent. Engineered nanomaterials offer unparalleled advantages, endowing enhanced chemical activity and stimulating photo-stimulated reaction at low power irradiation. Nanostructures are adsorbed by cytomembranes and lead to cell oxidation by protein denaturation, DNA damage, and ROS generation. Moreover, the size, morphology, and surface of nanostructures should be optimum to modify their ROS generation efficiency. In pursuit of high-performance nanostructured PSs, metal-based nanoparticles (e.g., gold nanostar and silver nanoparticles), metal–organic hybrid materials (e.g., TiO_2 and ZnO nanoparticles), hollow mesoporous silica nanoparticles, and MTSs, were reported [97–101].

Nanostructured MTSs can be used as phototherapy agents due primarily to their strong absorption in the NIR region, high extinction coefficients, versatile surface chemistry, high fluorescence, magnetism, structural, and thermal stability. MTSs are easily obtained through low-cost synthetic methods (compared to other NIR absorbing metal NPs), which can be scaled up to advance the reproducibility thereof. Investigations also show that MTSs can be utilized as PSs for PDT and nanocarriers for drug delivery due to their loading capacity, low degradation, long-time period, smart targeting, and formulated release. Besides their NIR absorbing capability due to metal-like plasma oscillation near NIR region, MTSs exhibit excellent photothermal conversion efficiency

under NIR irradiation, and currently are under extensive research. In the present review, different kinds of non-toxic nanostructured MTS PSs, including molybdenum disulfide, zinc sulfide, copper sulfide, iron sulfide, silver sulfide, bismuth sulfide, and cobalt sulfide, were comprehensively introduced and investigated for PDT, PTT, and chemotherapy applications. In these investigations, MTSs were typically coated with biocompatible polymers to mitigate the dark toxicity and to facilitate the interpenetration of cells and increased cell uptake under NIR irradiation. Among all their excellent properties, nanostructured MTSs were found to exhibit high absorption, Fenton reaction catalysis, innate photothermal and photodynamic response, controlled ROS production upon NIR irradiation, light source power dependent heat generation, and desired PDT efficiency. In most of these systems, photothermally enhanced PDT synergistic effect to treat solid tumors, induced photoablation of tumor cells and tissues, antitumor immune response, and great cell killing, and tumor inhibition capabilities were reported.

Despite all this progress, several persuading results and plenty of challenges (e.g., insignificant water solubility, photostability, and extended maintenance in tissues) limit the photodynamic clinical applications of MTSs. Biocompatibility, formulation, synthesis methods, and reliability of nanostructured MTSs must be carefully considered to further reduce the dark toxicity; improve the biodistribution, pharmacokinetics, clearance (after their therapeutic action), and discrimination between tumor and healthy tissues; and increase the upconversion efficiency. Functionalization of MTSs with specific target molecules to favor tumor accumulation should be also studied along with their degradation and metabolism. In this review, one of the main common limitations observed was the high laser power intensity, which in most cases was significantly higher than the clinically approved levels further restraining clinical translation. As for dose-limiting systematic toxicity of MTSs, no clear consensus has settled at least from the in vitro (mostly) and in vivo data covered in this review. In general, extensive research is continuously required to increase the PDT effectiveness and address these challenges. Taken altogether, to make PDT an interventional treatment and frontier method to fight against cancer, a critical and honest knowledge transfer from the different PDT-involved fields is desperately needed, with experts on this multidisciplinary topic effectively discussing the main hurdles and realistic opportunities.

Abbreviations

PDT: Photodynamic therapy; PS: Photosensitizer; ROS: Reactive oxygen species; PEG: Poly(ethylene glycol); $^1O_2$: Singlet oxygen; $^3O_2$: Molecular oxygen; PTT: Photothermal therapy; MTS: Metal transition sulfide; NMC: Nanostructured metal chalcogenide; S_1: Excited singlet state; T_1: Triplet excited state; NIR: Near infrared; LSPR: Localized surface plasmon resonance; PTCE: Photothermal conversion efficiency; RET: Resonance energy transfer; PDA: Polydopamine; BSA: Bovine serum albumin; MTX: Methotrexate; DPBF: 1,3-Diphenylisobenzofuran; EPR: Enhanced permeability and retention; CT: Computed tomography; QD: Quantum dot; ND: Nanodot; NP: Nanoparticle; NR: Nanorod; UCNP: Upconversion nanoparticle; FA: Folic acid; TEM: Transmission electron microscopy.

Acknowledgements

Not applicable.

Authors' Contributions

The manuscript was written by all authors, who reviewed and commented on the manuscript at all stages. All authors read and approved the final manuscript.

Funding

J.B-H acknowledges the startup funds provided by the East Carolina University through the Division of Research, Economic Development and Engagement (REDE), Thomas Harriot College of Arts and Sciences, and the Department of Physics.

Availability of Data and Materials

Not applicable.

Declarations

Competing interests

The authors declare that they have no competing interests.

Author details

[1]Department of Chemistry, University of Puerto Rico, San Juan, PR 00931, USA. [2]Present Address: NAMSA, 400 US Highway 169 S, Suite 500, Minneapolis, MN 55426, USA. [3]Department of Physics, Babol Noshirvani University of Technology, 47148 Babol, Iran. [4]Department of Physics, Alzahra University, 19938 Tehran, Iran. [5]Advanced Imaging Research Center, University of Texas Southwestern Medical Center, Dallas, TX 75390, USA. [6]Department of Physics, Howell Science Complex, East Carolina University, Greenville, NC 27858, USA.

Received: 22 December 2021 Accepted: 27 February 2022
Published online: 08 March 2022

References

1. Sung H, Ferlay J, Siegel RL et al (2021) Global cancer statistics 2020 GLOBOCAN estimates of incidence and mortality worldwide for 36 cancers in 185 countries. CA Cancer J Clin. https://doi.org/10.3322/caac.21660
2. Greshock J, Lewi M, Hartog B, Tendler C (2020) Harnessing real-world evidence for the development of novel cancer therapies. Trends Cancer 6:907–909. https://doi.org/10.1016/j.trecan.2020.08.006
3. Stegmeier F, Warmuth M, Sellers WR, Dorsch M (2010) Targeted cancer therapies in the twenty-first century lessons from imatinib. Clin Pharmacol Ther 87:543–552. https://doi.org/10.1038/clpt.2009.297
4. Nurgali K, Jagoe RT, Abalo R (2018) Editorial adverse effects of cancer chemotherapy anything new to improve tolerance and reduce sequelae? Front Pharmacol. https://doi.org/10.3389/fphar.2018.00245
5. Formenti SC, Demaria S (2009) Systemic effects of local radiotherapy. Lancet Oncol 10:718–726. https://doi.org/10.1016/S1470-2045(09)70082-8
6. Ng CSH, Lee TW, Wan S et al (2005) Thoracotomy is associated with significantly more profound suppression in lymphocytes and natural killer cells than video-assisted thoracic surgery following major lung resections for cancer. J Investig Surg 18:81–88. https://doi.org/10.1080/08941930590926320
7. Lucky SS, Soo KC, Zhang Y (2015) Nanoparticles in photodynamic therapy. Chem Rev 115:1990–2042. https://doi.org/10.1021/cr5004198
8. Castano AP, Demidova TN, Hamblin MR (2004) Mechanisms in photodynamic therapy part one—-photosensitizers, photochemistry and

cellular localization. Photodiagn Photodyn Ther 1:279–293. https://doi.org/10.1016/S1572-1000(05)00007-4
9. Castano AP, Mroz P, Hamblin MR (2006) Photodynamic therapy and anti-tumour immunity. Nat Rev Cancer 6:535–545. https://doi.org/10.1038/nrc1894
10. Allison RR, Moghissi K (2013) Photodynamic therapy (PDT) PDT mechanisms. Clin Endosc 46:24. https://doi.org/10.5946/ce.2013.46.1.24
11. Abrahamse H, Hamblin MR (2016) New photosensitizers for photodynamic therapy. Biochem J 473:347–364. https://doi.org/10.1042/BJ20150942
12. Chilakamarthi U, Giribabu L (2017) Photodynamic therapy past, present and future. Chem Rec 17:775–802. https://doi.org/10.1002/tcr.201600121
13. Huang Z (2005) A review of progress in clinical photodynamic therapy. Technol Cancer Res Treat 4:283–293
14. Chen D, Xu Q, Wang W et al (2021) Type I photosensitizers revitalizing photodynamic oncotherapy. Small 17:2006742. https://doi.org/10.1002/smll.202006742
15. Huang X, Sun X, Wang W et al (2021) Nanoscale metal–organic frameworks for tumor phototherapy. J Mater Chem B 9:3756–3777. https://doi.org/10.1039/D1TB00349F
16. Dolmans DEJGJ, Fukumura D, Jain RK (2003) Photodynamic therapy for cancer. Nat Rev Cancer 3:380
17. Calixto GMF, Bernegossi J, de Freitas LM et al (2016) Nanotechnology-based drug delivery systems for photodynamic therapy of cancer: a review. Molecules (Basel, Switzerland) 21:342. https://doi.org/10.3390/molecules21030342
18. Sun J, Kormakov S, Liu Y et al (2018) Recent progress in metal-based nanoparticles mediated photodynamic therapy. Molecules 23:1704. https://doi.org/10.3390/molecules23071704
19. Chen D, Zhong Z, Ma Q et al (2020) Aza-BODIPY-based nanomedicines in cancer phototheranostics. ACS Appl Mater Interfaces 12:26914–26925. https://doi.org/10.1021/acsami.0c05021
20. Ma Q, Sun X, Wang W et al (2021) Diketopyrrolopyrrole-derived organic small molecular dyes for tumor phototheranostics. Chin Chem Lett. https://doi.org/10.1016/j.cclet.2021.10.054
21. Kou J, Dou D, Yang L (2017) Porphyrin photosensitizers in photodynamic therapy and its applications. Oncotarget 8:81591–81603. https://doi.org/10.18632/oncotarget.20189
22. Xiao D, Qi H, Teng Y et al (2021) Advances and challenges of fluorescent nanomaterials for synthesis and biomedical applications. Nanoscale Res Lett 16:167. https://doi.org/10.1186/s11671-021-03613-z
23. Barata JFB, Neves MGPMS, Lacerda PSS et al (2022) Quantum dot phthalocyanine non-covalent assemblies—a review. Dyes Pigments 198:109931. https://doi.org/10.1016/j.dyepig.2021.109931
24. Zhao Y, Chen B-Q, Kankala RK et al (2020) Recent advances in combination of copper chalcogenide-based photothermal and reactive oxygen species-related therapies. ACS Biomater Sci Eng 6:4799–4815. https://doi.org/10.1021/acsbiomaterials.0c00830
25. Younis MR, He G, Qu J et al (2021) Inorganic nanomaterials with intrinsic singlet oxygen generation for photodynamic therapy. Adv Sci 8:2102587. https://doi.org/10.1002/advs.202102587
26. Mokwena MG, Kruger CA, Ivan M-T, Heidi A (2018) A review of nanoparticle photosensitizer drug delivery uptake systems for photodynamic treatment of lung cancer. Photodiagn Photodyn Ther 22:147–154. https://doi.org/10.1016/j.pdpdt.2018.03.006
27. Conte C, Maiolino S, Pellosi DS et al (2016) Polymeric nanoparticles for cancer photodynamic therapy. Top Curr Chem 370:61–112. https://doi.org/10.1007/978-3-319-22942-3_3
28. Tzerkovsky DA, Osharin VV, Istomin YP et al (2014) Fluorescent diagnosis and photodynamic therapy for C6 glioma in combination with antiangiogenic therapy in subcutaneous and intracranial tumor models. Exp Oncol 36:85–89
29. Allison RR (2013) Photodynamic therapy oncologic horizons. Future Oncol 10:123–124. https://doi.org/10.2217/fon.13.176
30. Yavari N, Andersson-Engels S, Segersten U, Malmstrom P-U (2011) An overview on preclinical and clinical experiences with photodynamic therapy for bladder cancer. Can J Urol 18:5778–5786
31. Kostovic K, Pastar Z, Ceovic R et al (2012) Photodynamic therapy in dermatology current treatments and implications. Coll Antropol 36:1477–1481
32. Kawczyk-Krupka A, Bugaj AM, Latos W et al (2015) Photodynamic therapy in colorectal cancer treatment the state of the art in clinical trials. Photodiagn Photodyn Ther 12:545–553. https://doi.org/10.1016/j.pdpdt.2015.04.004
33. Kim MM, Darafsheh A (2020) Light sources and dosimetry techniques for photodynamic therapy. Photochem Photobiol 96:280–294. https://doi.org/10.1111/php.13219
34. Plaetzer K, Krammer B, Berlanda J et al (2009) Photophysics and photochemistry of photodynamic therapy fundamental aspects. Lasers Med Sci 24:259–268. https://doi.org/10.1007/s10103-008-0539-1
35. Ochsner M (1997) Photophysical and photobiological processes in the photodynamic therapy of tumours. J Photochem Photobiol B 39:1–18. https://doi.org/10.1016/S1011-1344(96)07428-3
36. Zhu TC, Finlay JC (2008) The role of photodynamic therapy (PDT) physics. Med Phys 35:3127–3136. https://doi.org/10.1118/1.2937440
37. Jacques SL (2013) Optical properties of biological tissues a review. Phys Med Biol 58:R37–R61. https://doi.org/10.1088/0031-9155/58/11/R37
38. Algorri JF, Ochoa M, Roldán-Varona P et al (2021) Light technology for efficient and effective photodynamic therapy: a critical review. Cancers 13:3484. https://doi.org/10.3390/cancers13143484
39. Ma J, Jiang L (2001) Photogeneration of singlet oxygen (1O2) and free radicals (Sen*-, O2*-) by tetra-brominated hypocrellin B derivative. Free Radic Res 35:767–777
40. McDonald DM, Baluk P (2017) Imaging of angiogenesis in inflamed airways and tumors newly formed blood vessels are not alike and may be wildly abnormal. Chest 128:602S-608S. https://doi.org/10.1378/chest.128.6_suppl.602S-a
41. Abels C (2004) Targeting of the vascular system of solid tumours by photodynamic therapy (PDT). Photochem Photobiol Sci 3:765–771. https://doi.org/10.1039/B314241H
42. Kwiatkowski S, Knap B, Przystupski D et al (2018) Photodynamic therapy – mechanisms, photosensitizers and combinations. Biomed Pharmacother 106:1098–1107. https://doi.org/10.1016/j.biopha.2018.07.049
43. Steubing RW, Yeturu S, Tuccillo A et al (1991) Activation of macrophages by Photofrin II during photodynamic therapy. J Photochem Photobiol, B 10:133–145
44. Hendrzak-Henion JA, Knisely TL, Cincotta L et al (1999) Role of the immune system in mediating the antitumor effect of benzophenothiazine photodynamic therapy. Photochem Photobiol 69:575–581
45. Chatterjee DK, Fong LS, Zhang Y (2008) Nanoparticles in photodynamic therapy an emerging paradigm. Adv Drug Deliv Rev 60:1627–1637. https://doi.org/10.1016/j.addr.2008.08.003
46. Chen D, Wang Z, Dai H et al (2020) Boosting $O_2^{\bullet-}$ photogeneration via promoting intersystem-crossing and electron-donating efficiency of Aza-BODIPY-based nanoplatforms for hypoxic-tumor photodynamic therapy. Small Methods 4:2000013. https://doi.org/10.1002/smtd.202000013
47. Chen D, Yu Q, Huang X et al (2020) A highly-efficient type I photosensitizer with robust vascular-disruption activity for hypoxic-and-metastatic tumor specific photodynamic therapy. Small 16:2001059. https://doi.org/10.1002/smll.202001059
48. Montaseri H, Kruger CA, Abrahamse H (2021) Inorganic nanoparticles applied for active targeted photodynamic therapy of breast cancer. Pharmaceutics 13:296. https://doi.org/10.3390/pharmaceutics13030296
49. Yi G, Hong SH, Son J et al (2018) Recent advances in nanoparticle carriers for photodynamic therapy. Quant Imaging Med Surg 8:433–443. https://doi.org/10.21037/qims.2018.05.04
50. Goel S, Chen F, Cai W (2014) Synthesis and biomedical applications of copper sulfide nanoparticles from sensors to theranostics. Small 10:631–645. https://doi.org/10.1002/smll.201301174
51. Han L, Zhang Y, Chen X-W et al (2016) Protein-modified hollow copper sulfide nanoparticles carrying indocyanine green for photothermal and photodynamic therapy. J Mater Chem B 4:105–112. https://doi.org/10.1039/C5TB02002F
52. Fei W, Zhang M, Fan X et al (2021) Engineering of bioactive metal sulfide nanomaterials for cancer therapy. J Nanobiotechnol 19:93. https://doi.org/10.1186/s12951-021-00839-y
53. Zhu X, Ji X, Kong N et al (2018) Intracellular mechanistic understanding of 2D MoS_2 nanosheets for anti-exocytosis-enhanced synergistic cancer

therapy. ACS Nano 12:2922–2938. https://doi.org/10.1021/acsnano.8b00516
54. Chou SS, Kaehr B, Kim J et al (2013) Chemically exfoliated MoS_2 as near-infrared photothermal agents. Angew Chem Int Ed 52:4160–4164. https://doi.org/10.1002/anie.201209229
55. Liu T, Wang C, Cui W et al (2014) Combined photothermal and photodynamic therapy delivered by PEGylated MoS_2 nanosheets. Nanoscale 6:11219–11225. https://doi.org/10.1039/C4NR03753G
56. Jia L, Ding L, Tian J et al (2015) Aptamer loaded MoS_2 nanoplates as nanoprobes for detection of intracellular ATP and controllable photodynamic therapy. Nanoscale 7:15953–15961. https://doi.org/10.1039/C5NR02224J
57. Liu Y, Peng J, Wang S et al (2018) Molybdenum disulfide/graphene oxide nanocomposites show favorable lung targeting and enhanced drug loading/tumor-killing efficacy with improved biocompatibility. NPG Asia Mater 10:e458–e458. https://doi.org/10.1038/am.2017.225
58. Radisavljevic B, Radenovic A, Brivio J et al (2011) Single-layer MoS 2 transistors. Nat Nanotechnol 6:147–150
59. Lee C, Yan H, Brus LE et al (2010) Anomalous lattice vibrations of single- and few-layer MoS2. ACS Nano 4:2695–2700
60. Hersam MC (2015) The reemergence of chemistry for post-graphene two-dimensional nanomaterials. ACS Nano 9:4661–4663
61. Song C, Yang C, Wang F et al (2017) MoS_2-based multipurpose theranostic nanoplatform realizing dual-imaging-guided combination phototherapy to eliminate solid tumor *via* a liquefaction necrosis process. J Mater Chem B 5:9015–9024. https://doi.org/10.1039/C7TB02648J
62. Jin R, Yang J, Ding P et al (2020) Antitumor Immunity triggered by photothermal therapy and photodynamic therapy of a 2D MoS_2 nanosheet-incorporated injectable polypeptide-engineered hydrogel combinated with chemotherapy for 4T1 breast tumor therapy. Nanotechnology 31:205102
63. Xu J, Gulzar A, Liu Y et al (2017) Integration of IR-808 Sensitized upconversion nanostructure and MoS_2 nanosheet for 808 nm NIR light triggered phototherapy and bioimaging. Small 13:1701841. https://doi.org/10.1002/smll.201701841
64. Liu Y, Wei C, Lin A et al (2020) Responsive functionalized MoSe2 nanosystem for highly efficient synergistic therapy of breast cancer. Colloids Surf B 189:110820. https://doi.org/10.1016/j.colsurfb.2020.110820
65. Ghorbani J, Rahban D, Aghamiri S et al (2018) Photosensitizers in antibacterial photodynamic therapy an overview. Laser Ther 27:293–302
66. Wu Q, Chu M, Shao Y et al (2016) Reduced graphene oxide conjugated with CuInS2/ZnS nanocrystals with low toxicity for enhanced photothermal and photodynamic cancer therapies. Carbon 108:21–37
67. Diaz-Diestra D, Beltran-Huarac J, Bracho-Rincon DP et al (2015) Biocompatible ZnS: Mn quantum dots for reactive oxygen generation and detection in aqueous media. J Nanopart Res 17:461. https://doi.org/10.1007/s11051-015-3269-x
68. Martynenko IV, Kuznetsova VA, Orlova AO et al (2015) Chlorin e6–ZnSe/ZnS quantum dots based system as reagent for photodynamic therapy. Nanotechnology 26:55102
69. He S-J, Cao J, Li Y-S et al (2016) CdSe/ZnS quantum dots induce photodynamic effects and cytotoxicity in pancreatic cancer cells. World J Gastroenterol 22:5012
70. Xie Y, Chen W, Bertoni G et al (2017) Tuning and locking the localized surface plasmon resonances of CuS (Covellite) nanocrystals by an amorphous CuPdxS shell. Chem Mater 29:1716–1723. https://doi.org/10.1021/acs.chemmater.6b05184
71. Xie Y, Carbone L, Nobile C et al (2013) Metallic-like stoichiometric copper sulfide nanocrystals phase- and shape-selective synthesis, near-infrared surface plasmon resonance properties, and their modeling. ACS Nano 7:7352–7369. https://doi.org/10.1021/nn403035s
72. Liu Y, Liu M, Swihart MT (2017) Plasmonic copper sulfide-based materials: a brief introduction to their synthesis, doping, alloying, and applications. J Phys Chem C 121:13435–13447. https://doi.org/10.1021/acs.jpcc.7b00894
73. Tian Q, Tang M, Sun Y et al (2011) Hydrophilic flower-like CuS superstructures as an efficient 980 nm laser-driven photothermal agent for ablation of cancer cells. Adv Mater 23:3542–3547. https://doi.org/10.1002/adma.201101295
74. Wang S, Riedinger A, Li H et al (2015) Plasmonic copper sulfide nanocrystals exhibiting near-infrared photothermal and photodynamic therapeutic effects. ACS Nano 9:1788–1800. https://doi.org/10.1021/nn506687t
75. Li M, Wang Y, Lin H, Qu F (2019) Hollow CuS nanocube as nanocarrier for synergetic chemo/photothermal/photodynamic therapy. Mater Sci Eng C 96:591–598. https://doi.org/10.1016/j.msec.2018.11.020
76. Huang C-X, Chen H-J, Li F et al (2017) Controlled synthesis of upconverting nanoparticles/CuS yolk–shell nanoparticles for *in vitro* synergistic photothermal and photodynamic therapy of cancer cells. J Mater Chem B 5:9487–9496. https://doi.org/10.1039/C7TB02733H
77. Chang Y, Cheng Y, Feng Y et al (2018) Resonance energy transfer-promoted photothermal and photodynamic performance of gold-copper sulfide yolk-shell nanoparticles for chemophototherapy of cancer. Nano Lett 18:886–897. https://doi.org/10.1021/acs.nanolett.7b04162
78. Yuan Y, Wang L, Gao L (2020) Nano-sized iron sulfide structure, synthesis, properties, and biomedical applications. Front Chem. https://doi.org/10.3389/fchem.2020.00818
79. Akamatsu K, Takei S, Mizuhata M et al (2000) Preparation and characterization of polymer thin films containing silver and silver sulfide nanoparticles. Thin Solid Films 359:55–60. https://doi.org/10.1016/S0040-6090(99)00684-7
80. Kim B, Park C-S, Murayama M, Hochella MF (2010) Discovery and characterization of silver sulfide nanoparticles in final sewage sludge products. Environ Sci Technol 44:7509–7514. https://doi.org/10.1021/es101565j
81. Cao Y, Bernechea M, Maclachlan A et al (2015) Solution processed bismuth sulfide nanowire array core/silver sulfide shell solar cells. Chem Mater 27:3700–3706. https://doi.org/10.1021/acs.chemmater.5b00783
82. Ajiboye TO, Onwudiwe DC (2021) Bismuth sulfide based compounds: properties, synthesis and applications. Results Chem 3:100151. https://doi.org/10.1016/j.rechem.2021.100151
83. Lin S, Wang Y, Chen Z et al (2018) Biomineralized enzyme-like cobalt sulfide nanodots for synergetic phototherapy with tumor multimodal imaging navigation. ACS Sustain Chem Eng 6:12061–12069. https://doi.org/10.1021/acssuschemeng.8b02386
84. Ge Z-H, Zhao L-D, Wu D et al (2016) Low-cost, abundant binary sulfides as promising thermoelectric materials. Mater Today 19:227–239
85. Revia RA, Zhang M (2016) Magnetite nanoparticles for cancer diagnosis, treatment, and treatment monitoring recent advances. Mater Today 19:157–168
86. McBain SC, Yiu HHP, Dobson J (2008) Magnetic nanoparticles for gene and drug delivery. Int J Nanomed 3:169
87. Jin Q, Liu J, Zhu W et al (2018) Albumin-assisted synthesis of ultrasmall FeS_2 nanodots for imaging-guided photothermal enhanced photodynamic therapy. ACS Appl Mater Interfaces 10:332–340. https://doi.org/10.1021/acsami.7b16890
88. Li M, Lin H, Qu F (2020) FeS2@C-ICG-PEG nanostructure with intracellular O2 generation for enhanced photo-dynamic/thermal therapy and imaging. Chem Eng J 384:123374. https://doi.org/10.1016/j.cej.2019.123374
89. Wang G, Liu J, Zhu L et al (2019) Silver sulfide nanoparticles for photodynamic therapy of human lymphoma cells via disruption of energy metabolism. RSC Adv 9:29936–29941
90. Cheng K, Zhang X, An J et al (2019) Hitherto-unexplored photodynamic therapy of Ag_2S and enhanced regulation based on polydopamine in vitro and vivo. Chem Eur J 25:7553–7560. https://doi.org/10.1002/chem.201900718
91. Faghfoori MH, Nosrati H, Rezaeejam H et al (2020) Anticancer effect of X-Ray triggered methotrexate conjugated albumin coated bismuth sulfide nanoparticles on SW480 colon cancer cell line. Int J Pharm 582:119320
92. Cheng Y, Chang Y, Feng Y et al (2019) Bismuth sulfide nanorods with retractable zinc protoporphyrin molecules for suppressing innate antioxidant defense system and strengthening phototherapeutic effects. Adv Mater 31:1806808. https://doi.org/10.1002/adma.201806808
93. Song X-R, Wang X, Yu S-X et al (2015) Co_9Se_8 nanoplates as a new theranostic platform for photoacoustic/magnetic resonance dual-modal-imaging-guided chemo-photothermal combination therapy. Adv Mater 27:3285–3291. https://doi.org/10.1002/adma.201405634
94. Zhou B, Shi B, Jin D, Liu X (2015) Controlling upconversion nanocrystals for emerging applications. Nat Nanotechnol 10:924–936. https://doi.org/10.1038/nnano.2015.251

95. Fan W, Huang P, Chen X (2016) Overcoming the Achilles' heel of photodynamic therapy. Chem Soc Rev 45:6488–6519. https://doi.org/10.1039/C6CS00616G
96. Kachynski AV, Pliss A, Kuzmin AN et al (2014) Photodynamic therapy by in situ nonlinear photon conversion. Nat Photonics 8:455–461. https://doi.org/10.1038/nphoton.2014.90
97. Xiao L, Gu L, Howell SB, Sailor MJ (2011) Porous silicon nanoparticle photosensitizers for singlet oxygen and their phototoxicity against cancer cells. ACS Nano 5:3651–3659. https://doi.org/10.1021/nn1035262
98. Yu Z, Zhou P, Pan W et al (2018) A biomimetic nanoreactor for synergistic chemiexcited photodynamic therapy and starvation therapy against tumor metastasis. Nat Commun 9:5044. https://doi.org/10.1038/s41467-018-07197-8
99. Zhang L, Yang X-Q, Wei J-S et al (2019) Intelligent gold nanostars for in vivo CT imaging and catalase-enhanced synergistic photodynamic & photothermal tumor therapy. Theranostics 9:5424–5442. https://doi.org/10.7150/thno.33015
100. El-Hussein A, Mfouo-Tynga I, Abdel-Harith M, Abrahamse H (2015) Comparative study between the photodynamic ability of gold and silver nanoparticles in mediating cell death in breast and lung cancer cell lines. J Photochem Photobiol, B 153:67–75. https://doi.org/10.1016/j.jphotobiol.2015.08.028
101. Zhang H, Shan Y, Dong L (2014) A comparison of TiO_2 and ZnO nanoparticles as photosensitizers in photodynamic therapy for cancer. J Biomed Nanotechnol 10:1450–1457. https://doi.org/10.1166/jbn.2014.1961

Publisher's Note